## Beamline 7.3.3

# X-Ray Microdiffraction

### Deciphering Ni sequestration in soil ferromagnanese nodules by combining x-ray fluorescence, absorption and diffraction at micrometer scales of resolution

Manceau, A., M.A. Marcus, N. Tamura, R.S. Celestre, A.A. MacDowell, R.E. Sublett, H.A. Padmore

### Determining trace metal speciation in soils at molecular-scale by combined x-ray fluorescence, diffraction and absorption

Manceau, A., N. Tamura, R.S. Celestre, A.A. MacDowell, G. Sposito, H.A. Padmore

### Experimental assessment of strain gradient plasticity theories

Barney, M.M., G.H. Campbell, J.S. Stölken, W.E. King, R.O. Ritchie

### High resolution study of the thermomechanical behavior of Al(0.5wt% Cu) thin films by scanning x-ray microdiffraction (μSXRD)

Tamura, N., B.C. Valek, R. Spolenak, R.S. Celestre, A.A. MacDowell, H.A. Padmore, B.W. Batterman, J.R. Patel

### In-situ synchrotron x-ray microdiffraction study of deformation behavior in copper-polycrystals during uniaxial deformations

Joo, H.D., J.S. Kim, K.H. Kim, N. Tamura, Y.M. Koo

### Local plasticity in Al(0.5wt% Cu) membranes revealed by scanning x-ray microdiffraction (μSXRD)

Spolenak, R., N. Tamura, B.C. Valek, R.S. Celestre, A.A. MacDowell, H.A. Padmore, W.L. Brown, B.W. Batterman, J.R. Patel

### Macro stress mapping on thin film buckling

Goudeau, P., P. Villain, N. Tamura, R.S. Celestre, H. Padmore

### Microstructure and pinning properties of hexagonal-disc shaped single crystalline $MgB_2$

Jung, C.U., J.Y. Kim, P. Chowdhury, K.H.P. Kim, S.-I. Lee, N. Tamura, W.A. Caldwell, J.R. Patel

### Monitoring anthropogenic metal released in the environment via x-ray fluorescence, absorption and diffraction at micrometer scales of resolution

Manceau, A., M.A. Marcus, N. Tamura, R.S. Celestre, A.A. MacDowell, R.E. Sublett, H.A. Padmore, M. Kersten

### Strain and stress in a thin film $YBa_2Cu_3O_x$ bicrystal grain boundary on $SrTiO_3$ substrate studied by x-ray micro-diffraction

Caldwell, W.A., N. Tamura, R.S. Celestre, A.A. MacDowell, H.A. Padmore, J.R. Patel

# Deciphering Ni sequestration in soil ferromanganese nodules by combining X-ray fluorescence, absorption and diffraction at micrometer scales of resolution

A. Manceau[1,2], M.A. Marcus[1], N. Tamura[1], R.S. Celestre[1], A.A. MacDowell[1], R.E. Sublett[1], H.A. Padmore[1]
[1]Advanced Light Source, Lawrence Berkeley National Laboratory, Berkeley, CA 94720
[2]Environmental Geochemistry Group, Hilgard Hall, University of California, Berkeley, CA 94720

Soils are a major sink for anthropogenic Ni, and its migration to living organisms is an environmental concern because of its suspected carcinogenicity when it is speciated as nickel sulfate or combinations of nickel sulfides and oxides, provoking lung and nasal cancers. The anthropogenic nickel sources are the metal processing operations, the combustion of coal and oil, and amendments by sewage sludge. The crystal chemistry of nickel in oxidized and silicated ores has been abundantly studied for economic reasons, and in these formations Ni is predominantly associated with phyllosilicates and the Fe oxyhydroxide, goethite (α-FeOOH). During its journey from the source to its resting place in soils, Ni can undergo many chemical transformations, and understanding how this element is naturally sequestered helps provide a solid scientific basis for maintaining soil quality and formulating educated strategies to remediate severely impacted areas. The most efficient and durable process responsible for trace metal sequestration in soils is the formation of ferromanganese micronodules, which often have been compared to the well-known oceanic Mn nodules. In this work, we have studied how nickel is sequestered in soil nodules from the Morvan region (France) by combining, for the first time, scanning X-ray microfluorescence (μSXRF), microdiffraction (μSXRD), and extended X-ray absorption fine structure (μEXAFS) spectroscopy, all applied at the micrometer-scale of resolution. The two first techniques were used to identify the host solid phase by mapping the distributions of elements and solid species, respectively. μEXAFS was then used to determine the mechanism of Ni binding by the host phase at the molecular scale. We showed that nickel substitutes for $Mn^{3+}$ in the manganese layer of the $MnO_2$-$Al(OH)_3$ mixed-layer oxide lithiophorite. The affinity of Ni for this mineral was subsequently found to be characteristic of micronodules sampled from soils across the USA and Europe. Since many natural and synthetic materials are heterogeneous at nanometer to micrometer scales, the unprecedented synergistic use of μSXRF, μSXRD, and μEXAFS is expected to have broad applications to earth and materials science.

## RESULTS AND INTERPRETATION

With μSXRF (three first maps) the distribution of Fe, Mn, and Ni were first determined, and it was found that Mn and Ni were systematically associated in the six different soil nodules examined in this study. Then, mineral abundance maps were produced by integrating at each point-of-analysis the diffracted intensities of the non-overlapping (020) and (200) reflections at ~4.45 Å and ~2.57 Å for phyllosilicate, the (101) and (301) reflections at 4.19 Å and 2.69 Å for goethite, the (001) reflection at 7.1-7.2 Å for birnessite, and the (001) and (002) reflections at 9.39 Å and 4.69 Å for lithiophorite. The reliability of this quantitative treatment was verified by comparing mineral maps calculated using independent (*hkl*) reflections of the same mineral species. The distribution of Fe-vernadite, a common soil mineral, was not mapped because it was systematically detected throughout the examined nodules without significant gradient of concentration. This Fe-Mn disordered phase (also termed Mn-feroxyhite), that is dispersed throughout the nodule matrix filling pores and aggregating coarse grains, acts as a cementing agent for the nodules.

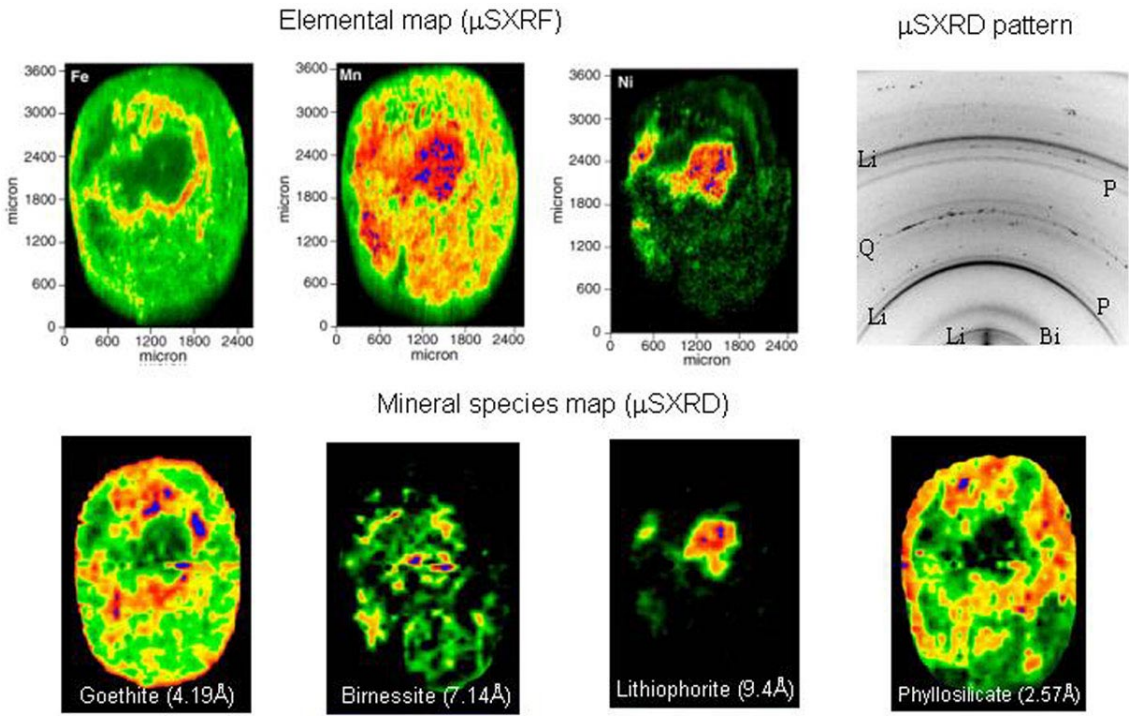


Figure 1. Combined fluorescence - diffraction measurements recorded at Beamline 7.3.3. on a ferromanganese soil nodule. The three images on the top are elemental maps obtained by µSXRF, and the four images on the bottom are mineral species maps obtained by integrating at each point of analysis the intensities of the relevant (*hkl*) reflections along the Debye rings of the two-dimensional XRD patterns (d-spacings are indicated in parenthesis). One XRD pattern is presented to the top right. Li = lithiophorite, Bi = birnessite, P = phyllosilicate, Q = quartz.

The comparison of the µSXRF and µSXRD maps clearly shows that nickel and lithiophorite have the same contour maps, therefore suggesting that Ni is bound to this particular mineral phase. The systematic association of Ni-lithiophorite suggests that Ni should be located in a definite cation site of the manganese oxide crystal structure. To determine the Ni site, Ni K-edge µEXAFS spectra were collected on Beamline 10.3.2. in Ni 'hot spots' from several nodules. All spectra were identical, indicating that the incorporation mechanism of nickel is unique, and is the key to understanding its sequestration in soils. Qualitative information about the local structure of Ni can be obtained by comparing the unknown µEXAFS spectrum to reference EXAFS spectra from relevant model compounds. As expected from µSXRF – µSXRD experiments, the two reference spectra for Ni in goethite and phyllosilicate did not match the unknown spectrum, confirming that Ni is not sequestered in these forms (data not shown). Differences in frequency and shape of the EXAFS oscillations were also observed with birnessite, in which Ni is sorbed above vacant Mn sites, and with lithiophorite, in which Ni is located within the gibbsitic Al layer (Fig. 2a). The radial structure functions (RSFs) obtained by Fourier transforming EXAFS spectra for the reference and the soil lithiophorite both exhibit, after the first oxygen peak, a second peak at roughly $R + \Delta R = 2.6$ Å, that is at a distance characteristic of edge-sharing linkage between metal octahedra (Fig. 2b). This result alone suggests that Ni is located within one of the two octahedral layers of the lithiophorite structure. To solve this alternative, suffice it to examine the phase of the imaginary part of the Fourier transform, because waves backscattered by Al and Mn atoms are almost out-of-phase. Examination of Fig. 2c shows that the unknown and lithiophorite reference have their electronic waves shifted by $\sim\pi$ in the 2.2 – 3.1 Å $R + \Delta R$ interval, thus indicating that Ni is substituted for Mn in the soil lithiophorite. In keeping with this conclusion, the two waves

are logically in phase in the 1.0 – 2.2 Å R + ΔR interval, since in both structures Ni is octahedrally coordinated to oxygen atoms.

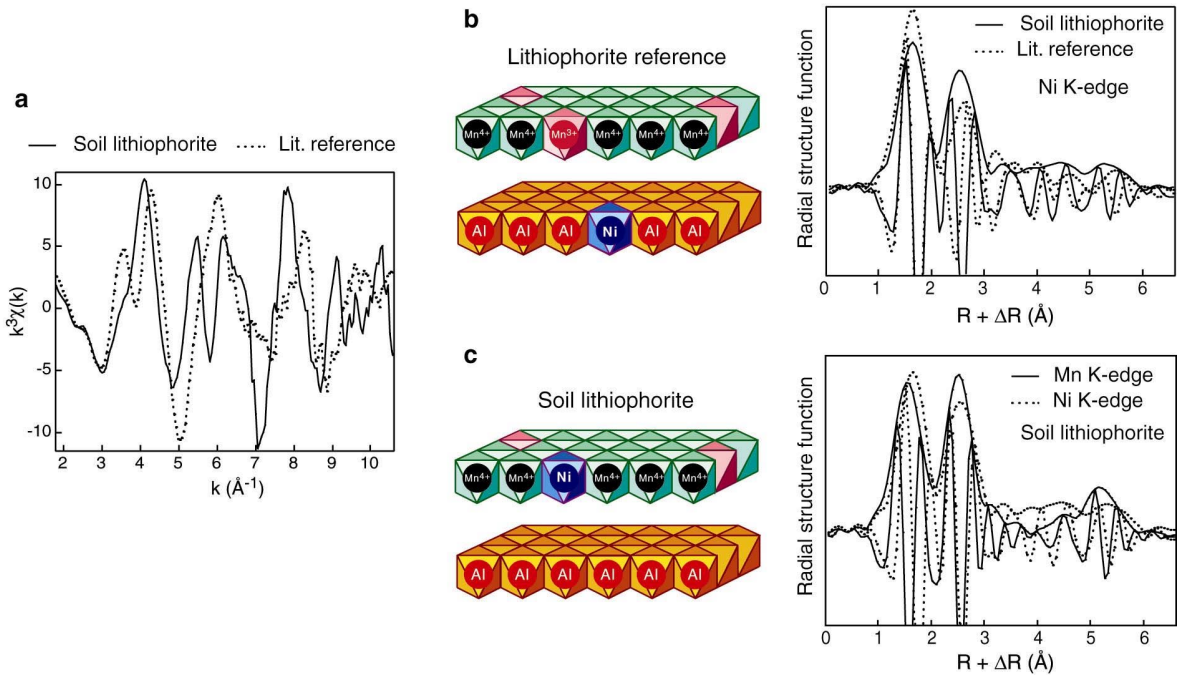


Figure 2. Ni K-edge μEXAFS spectrum (**a**) and Fourier transform (modulus plus imaginary part) (**b,c**) from a 'hot spot' of the core of the nodule, compared to the Ni- and Mn-edge data from a Ni-containing lithiophorite reference, in which Ni substitutes for Li in the $Al(OH)_3$ layer. Data were collected on Beamline 10.3.2.

Since $Ni^{2+}$ has an effective radii 30% greater than $Mn^{4+}$, one may wonder how the Ni-Mn substitution is realized. To answer this question, Ni- and Mn-RSFs were plotted together (Figure 2b, bottom right), and the Ni- and Mn-EXAFS interatomic distances compared. A distinct feature in the Ni-RSF is the shift to higher R + ΔR values of the Ni-O peak, indicative of a relaxation of the Ni site owing to the larger ion size of the $Ni^{2+}$ impurity ($r$ = 0.69 Å) relative to $Mn^{4+}$ ($r$ = 0.53 Å) and $Mn^{3+}$ ($r$ = 0.645 Å). Since $Ni^{2+}$ and $Mn^{3+}$ have a size mismatch of only 7%, nickel likely substitutes on the trivalent manganese site. Likewise, the $Al^{3+}$ site of the gibbsitic layer is clearly too small ($r$ = 0.535 Å) to accommodate $Ni^{2+}$, and the larger $Li^{+}$ site ($r$ = 0.76 Å) is probably energetically less favorable. This assumption is supported by recent atomistic calculations and EXAFS measurements on lanthanide-doped perovskite, which showed that the rare earth is energetically stabilized in smaller crystallographic sites. A best fit to our data was given by octahedral coordination of nickel with oxygen at 2.05 Å and six manganese at 2.91 Å, and average Mn-O and Mn-Mn distances of 1.92 Å and 2.92 Å, respectively. There was no indication of Ni-Ni pairs, for which Ni-Ni distances of 3.03 Å to 3.12 Å would be predicted. This result indicates that nickel did not precipitate as a hydroxide, hence confirming that the next-nearest coordination shell of Ni is made of Mn atoms. Similar results were obtained on nodules from flood plain soils in the USA, which suggests that the Ni species identified herein may correspond to a major sequestration form of Ni in Earth near-surface environments.

This work was supported by the LBNL Laboratory Director's Research and Development Fund and by the US Department of Energy, Office of Basic Energy Sciences, under contract # DOE-AC03-765F00098.

Principal investigator: Alain Manceau, Advanced Light Source, Ernest Orlando Lawrence Berkeley National Laboratory. Email: acmanceau@lbl.gov. Telephone: 510-643-2324.

# Determining trace metal speciation in soils at molecular-scale by combined X-ray fluorescence, diffraction and absorption

A. Manceau[1,2], N. Tamura[1], R.S. Celestre[1], A.A. MacDowell[1], G. Sposito[2], H.A. Padmore[1]
[1] Advanced Light Source, Lawrence Berkeley National Laboratory, Berkeley, California 94720, USA
[2] ***Environmental Geochemistry Group, Hilgard Hall, University of California, Berkeley, CA 94720, USA***

## INTRODUCTION

Understanding how environmentally-important trace metals are sequestered in soils at the molecular scale is critical to developing a solid scientific basis for maintaining soil quality and formulating effective strategies to remediate severely contaminated areas. The speciation of Zn and Ni in flood plain soils was determined by a novel synergistic use of three non-invasive synchrotron-based techniques, X-ray microfluorescence (μSXRF); X-ray microdiffraction (μXRD); and extended X-ray absorption fine structure spectroscopy (EXAFS). Eight nodules from the Mississippi basin were examined by μSXRF and μXRD on the 7.3.3. microdiffraction beamline, and complementary EXAFS measurements were performed at the European Synchrotron Radiation Facility in Grenoble (France). Here, only the first set of results is presented.

## RESULTS AND INTERPRETATION

The chemical composition of the nodules was determined using inductively coupled plasma atomic emission spectroscopy (ICP-AES) and inductively coupled plasma mass spectroscopy (ICP-MS). These analyses gave [Fe] = 57526 ($\sigma$ = 21213), [Mn] = 25592 ($\sigma$ = 17716), [Zn] = 76 ($\sigma$ = 51), [Ni] = 67 ($\sigma$ = 21) mg/kg. The $\sigma$ variability of the bulk analyses is relatively low, and contrasts with the μSXRF maps, which show that individual nodules are highly heterogeneous at the micrometer scale, containing distinct areas of concentrated Fe, Mn, Ni and Zn (Fig. 1).

The mineralogy and crystal chemistry of Zn and Ni in the series of nodules is completely represented by the three samples in Fig. 1. Nodule 1 shows, on average, little correlation between Fe and Mn ($r_{Fe-Mn}$= 0.62), but visual inspection of the maps shows that the degree of correlation varies laterally. The richest Fe areas in the outer region are strongly depleted in Mn, whereas the inner region contains areas of both high Mn and high Fe. Zn and Ni are strongly correlated with Fe ($r_{Fe-Zn}$ = 0.84, $r_{Fe-Ni}$ = 0.88) and, to a lesser extent, with Mn ($r_{Mn-Zn}$ = 0.71, $r_{Mn-Ni}$ = 0.78). The relatively high $r_{Mn-Ni}$ value does not necessarily indicate that a Ni fraction is actually associated with Mn, but instead can result from the incomplete separation of Fe and Mn in the core of a nodule. μXRD patterns were collected with a CCD camera at different points selected on the elemental maps. The outermost Fe-rich region was found to consist of finely-dispersed goethite ($\alpha$–FeOOH). Quartz, feldspar, titanium oxide, and carbonate grains also were detected. The Fe-Mn core consists of either Mn-feroxyhite ($\delta$-FEOOH) or Fe-vernadite ($\delta$-$MnO_2$), depending on the Fe/Mn ratio. Therefore, Zn and Ni appear to be predominantly bound to goethite in this nodule.

Mn, Fe, Zn, and Ni were also unevenly distributed in nodule 2 (Fig. 1b), which showed a moderate overall correlation between Fe and Mn ($r_{Fe-Mn}$ = 0.78). However, the central region is high in Fe and Mn, whereas the external Fe layer is depleted in Mn. As with the previous nodule, this result illustrates the spurious meaning of elemental correlations calculated solely from total chemical analyses. Nodule 2 possesses a Zn-Ni "hot spot", about 80 x 80 $\mu m^2$ in area, which is strongly

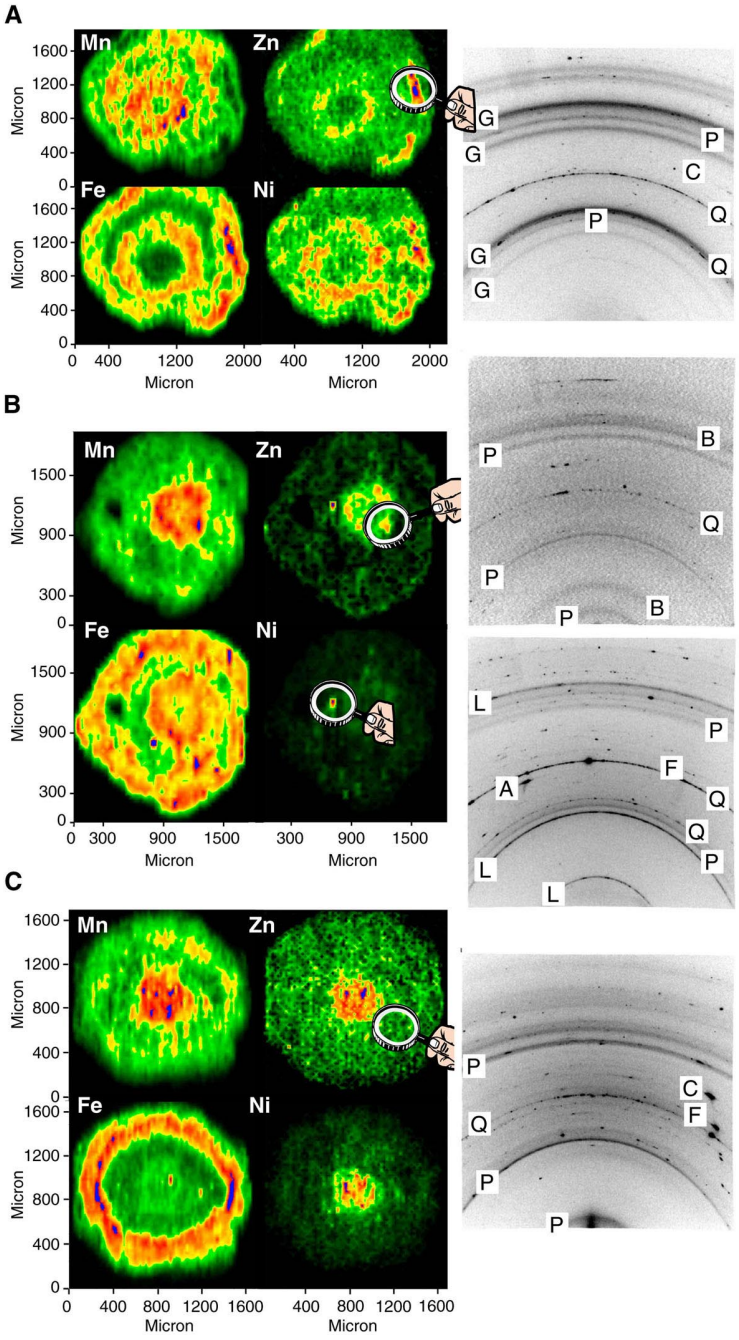


Figure 1. Synchrotron-based micro-X-ray fluorescence (µSXRF) maps obtained by scanning soil nodules under a monochromatic beam (E = 10 keV; beam size on the sample: 10 µm H x 25 µm V; step size: 32 x 32 µm (a), 42 x 42 µm (b), 25 x 25 µm (c); counting time: 5 to 8 s/point). µXRD patterns were collected at selected points of interest using a 1024 x 1024 pixels CCD camera and an exposure time of 10 to 20 min (E= 6.0 keV (a, b) and 6.3 keV (c)). All data were collected in reflection geometry mode by inclining the sample at 6° θ. B = hexagonal birnessite (main diffraction peaks at 7.1-7.2 Å, 2.45 Å, and 1.41 Å), G = goethite (main diffraction peaks at 4.18 Å and 2.69 Å), L = lithiophorite (main diffraction peaks at 9.4 Å, 4.7 Å, and 2.37 Å), P = phyllosilicate (main diffraction peaks at 4.45-4.48 Å, 2.55–2.58 Å, and 1.50 Å). In (a) Ni and Zn are associated with goethite (α-FeOOH); in (b) Ni is associated with lithiophorite, and Zn with lithiophorite and birnessite; in (c) Ni is associated with lithiophorite and Zn with lithiophorite and phyllosilicate.

correlated with Mn. The core of the nodule is enriched in Zn as well, but devoid of Ni, suggesting that nodule 2 contains two major Zn species, but only a single Ni species, one which also contains Zn. The mineralogical nature of the minute Mn grain containing both Zn and Ni was identified by µXRD as lithiophorite, a $MnO_2$ - $Al(OH)_3$ mixed-layer phyllomanganate (Fig. 2). In the two-dimensional XRD pattern, Bragg reflections from this grain formed a continuous Debye ring, characteristic of a powder diffraction pattern. The lithiophorite is, therefore, very fine-grained like most natural reactive particles. Randomly-layered birnessite (also termed vernadite), together with phyllosilicate, was positively identified in the central region by µXRD (Fig. 1b). Vernadite and lithiophorite are considered to be the two predominant Mn mineral species in near-surface environments, but their defective structure (vernadite) and small particle size pose major problems for identifying them by conventional XRD. The combination of µSXRF and µXRD provides the necessary lateral resolution for establishing their presence and role in the sequestration of trace metals.

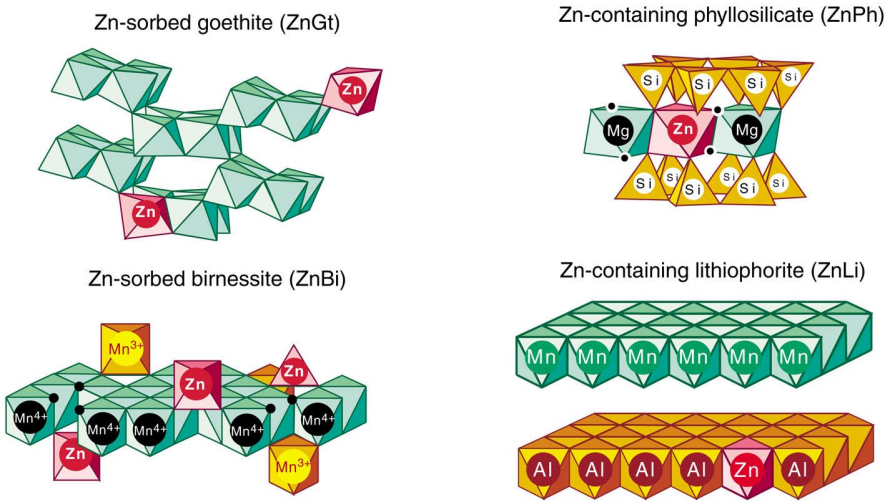


Figure 2. Structure of minerals in which Zn and Ni are sequestered.

Two Zn fractions were also detected in nodule 3 (Fig. 1c). In the first, Zn is concentrated with Ni and Mn at the core, which, according to µXRD, contains lithiophorite and phyllosilicate, a geochemical association already found in nodule 2. The second fraction of Zn has a uniform background signal distributed throughout the nodule and likely as well in the central region, where it is masked by the Zn,Ni lithiophorite species. Clearly, this second Zn fraction is not bound either to Fe or Mn oxides, because neither the Fe nor the Mn map shows areal contours similar to the Zn map. µXRD patterns collected in Zn-containing (but Fe- and Mn-depleted) regions showed the presence of dioctahedral phyllosilicates (Fig. 1c). Therefore, the second Zn fraction likely corresponds to a Zn-containing phyllosilicate. It was almost impossible to find regions containing only Fe or Mn oxides. For example, the four two-dimensional µXRD patterns presented in Fig. 1 all contain diffraction rings at 4.45-4.48 Å and 2.55-2.58 Å, typical of the 020-110 and 130-200 reflections that characterize sheet silicates. A peak at 1.50 Å was observed systematically at higher diffraction angles, thus indicating the mostly dioctahedral structure of these minerals. Elemental correlation coefficients for nodule 3 can be interpreted readily based on these results. Little correlation was obtained for Fe and Mn ($r_{Fe\text{-}Mn}$=0.69), in agreement with the nonoverlapping contour maps for these two elements. The Mn-Zn correlation is moderate ($r_{Mn\text{-}Zn}$=0.76) owing to

the partial association of Zn with phyllosilicate, whereas the Mn-Ni correlation is strong ($r_{Mn-Ni}$=0.82) since Ni is uniquely bound to lithiophorite. Correlations between Fe and Zn ($r_{Fe-Zn}$=0.44) or Fe- and Ni ($r_{Fe-Ni}$=0.33) are low, as expected.

In summary, μSXRF and μXRD microanalyses showed that Zn is bound to four mineral species, goethite, phyllosilicate, hexagonal birnessite, and lithiophorite, whereas nickel is sequestered by goethite and lithiophorite. This difference in speciation of Zn and Ni provides a clue to the observed higher partitioning of Ni in the soil nodules over the soil matrix. Nodules commonly form in soils with restricted internal drainage by the solubilisation of Fe(II) and Mn(II) under reducing conditions, followed by precipitation as Fe(III) and Mn(III,IV) oxides under oxidising conditions. Consequently, concretions have the same quantities of phyllosilicates and coarse grains (quartz, feldspar, titanium oxides…) as does the soil matrix, but they contain a higher quantity of finely-divided Fe and Mn oxides that cement soil material together and reduce its porosity. Since Zn is predominantly speciated as a phyllosilicate (EXAFS data not shown), and because this latter mineral is uniformly present in the soil, Zn partitioning in nodules is necessarily limited. The high Ni partitioning into the nodules results directly from selective sequestration by Fe and Mn oxides, the principal minerals that cause nodule formation. Thus, the novel combination of μSXRF, μXRD, and EXAFS spectroscopy provides the approach needed to speciate metals in a natural matrix not possible to study accurately with conventional techniques.

This work was supported by the LBNL Laboratory Director's Research and Development Fund and by the US Department of Energy, Office of Basic Energy Sciences, under contract # DOE-AC03-765F00098.

Principal investigator: Alain Manceau, Advanced Light Source, Ernest Orlando Lawrence Berkeley National Laboratory. Email: acmanceau@lbl.gov. Telephone: 510-643-2324.

# Experimental assessment of strain gradient plasticity theories

M.M. Barney[1, 2], G.H. Campbell[2], J. S. Stölken[2], W.E. King[2], R.O. Ritchie[1]
[1] Lawrence Berkeley National Laboratory, University of California, Berkeley, California 94720, USA
[2] Lawrence Livermore National Laboratory, University of California, Livermore, California 94551, USA

## INTRODUCTION

Classical plasticity theories generally assume that the stress at a point is a function of strain at that point only. However, when gradients in strain become significant, this localization assumption is no longer valid. These conventional models fail to display a 'size effect'. This effect is seen experimentally when the dimension characteristic of the physical phenomenon involved is on the order of the microstructural scale of interest. Under these conditions, strain gradients are of a significant magnitude as compared to the overall strain and must be considered for models to accurately capture observed behavior.

The mechanics community has been actively involved in the development of strain gradient theories for many years. Recently, interest in this area has been rekindled and several new approaches have appeared in the literature. Two different approaches are currently being evaluated. One approach considers strain gradients as internal variables that do not introduce work conjugate higher order stresses. Another approach considers the strain gradients as internal degrees of freedom that requires work conjugate higher order stresses. Experiments are being performed to determine which approach models material behavior accurately with the least amount of complexity. A key difference between the two models considered here is the nature of the assumed boundary conditions at material interfaces. Therefore, we are investigating the deformation behavior of metal/sapphire interfaces loaded under simple shear. To determine the lattice rotations near the boundary, we are examining the samples with submicron X-ray methods and with diffraction techniques in the transmission electron microscope. The experimentally found boundary conditions shall be subsequently used to determine whether the simpler internal variable model is adequately descriptive. This information will also be included in the mesoscale simulations to be carried out as part of the LLNL Multiscale Materials Modeling Project.

## BACKGROUND

Although not predicted by classical models, an increase in flow stress is seen during deformation when the observed phenomena is on the order of a micron and inhomogeneties are present. For example, Fleck et.al. [1] showed that when loaded in torsion, a wire displays greater strength for smaller radii. Others authors have observed this type of effect in other systems, including bending [2], indentation hardness [3], and particle hardened alloys [4]. The increase in hardness under these conditions is attributed to the additional dislocations needed for compatibility. These dislocations are commonly referred to as geometrically necessary dislocations [5]. The presence of these dislocations can be ignored and continuum theories applied at large size scales since gradients in strain are small. However, at smaller size scales, more dislocations are formed in a smaller area, resulting in large strain gradients and higher flow stresses. When strain gradients become significant, this localization assumption in continuum theories is no longer valid [6]. This must be accounted for in a non-local theory to accurately reflect material response. Two distinct classes of models that extend classical theories to include strain gradient effects are currently being evaluated. Fleck and Hutchinson [7] have developed one approach (referred to as the FHS model [8]) that considers strain gradients as internal degrees of freedom and requires thermodynamic work conjugate higher order stresses, which need additional boundary conditions. Acharya and Bassani [9] have developed an alternative approach in which a strain gradient term is included in the hardening function. In this method, the strain gradients are considered to be internal variables, which do not introduce higher order stresses or additional boundary conditions. This approach has the advantages that it is simpler overall, preserves the structure of the classical boundary value problem, and can easily be implemented into existing finite element codes. However, the higher order theory may be more predictive because it allows for constraints on strain to be enforced at interfaces. The additional boundary conditions in the higher order theory allow for the presence of a

boundary layer. Specifically, Fleck and Hutchinson [7] determined theoretically that a boundary layer of lattice rotation should be present at an interface between dissimilar materials loaded under remote simple shear. Since boundary layers are not predicted in Acharya and Bassani's approach, detecting the presence of these layers at interfaces will supply critical information in the continued development of strain gradient plasticity theories. Boundary layers seem likely in real materials, since stress fields that are strongly affected by boundaries [10] govern dislocation motion. The presence of a boundary layer, however, has not yet been definitively determined. Although previous experimental work on bicrystals by Sun et.al [11] suggests the presence of a boundary layer, the data are difficult to interpret due to the movement of the grain boundary. Therefore, experiments performed at a metal-ceramic interface are proposed to determine deformation behavior without the complication of grain boundary movement.

## EXPERIMENTAL PROCEEDURE

The deformation behavior near an interface is investigated using samples composed of 25μm thick aluminum foils sandwiched between sapphire rods (see [12] for more details). An ultra-high vacuum diffusion-bonding machine [13] is used to bond the two materials. The metal layer is sheared using asymmetric four point bending. This test is used to achieve a uniform simple shear stress state. This stress state is needed to shed light on existing strain gradient models, because each model considered predicts different behavior under this condition. Finite element modeling is used to simulate this experiment in order to confirm the homogeneity of the deformation. The sapphire is modeled as an isotropic elastic material and the metal is modeled as a $J_2$ linear hardening material. The modeling confirms that the metal layer is under a homogeneous stress state, but does exhibit some edge effects in the strain profiles. This will not affect the experimental results, because observations are only made in the center of the sample.

In order to detect the presence of a boundary layer in the aluminum near the sapphire, the lattice rotations need to be measured from the center of the aluminum layer to an interface in one micron steps. To measure the rotation, the mechanically tested samples were cut into slices for observation of diffraction patterns in a transmission electron microscope (TEM). Unfortunately, standard TEM sample preparation methods cause the aluminum to recrystallize, so a non-destructive method is desired. Unlike most X-ray techniques, the submicron X-ray technique developed at the Advanced Light Source (ALS) [14] uses a small enough spot size to properly investigate the lattice rotation changes in these samples. Unfortunately, the noise from the surface damage layer formed during the polishing of the aluminum is obscuring the signal from the Laue patterns in the bulk region. It has not been possible to fully analyze this data. From some initial analysis, there does appear to be a measurable change in lattice rotation as the interface is approach. However, improved sample preparation techniques to produce a stronger signal need to be employed to confirm this initial indication. Confirming or refuting the presence of this boundary layer is the primary result of the experimental program. If the boundary layer is present, its characterization will be critical in providing parameters for the FHS model. Continued improvement of the model will be facilitated by further experimental results generated by continued investigations. The cyclic feedback of information between experiments and modeling has proven to be successful in other parts of the Multiscale Materials Modeling Project at Lawrence Livermore National Laboratory.

## ACKNOWLEDGMENTS

The authors would like to thank Dr. Ralph Spolenak and Dr. Nobumichi Tamura for assistance with the ALS beamline 7.3.3 and for data analysis.

## REFERENCES

1. N. A. Fleck, G. M. Muller, M. F. Ashby, and J. W. Hutchinson, Acta Metall. Mater. **42**, 475 (1993).
2. J. S. Stölken and A. G. Evans, Acta. Mater. **46**, 5109 (1998).

3. N. A. Stelmashenko, M. G. Walls, L. M. Brown, and Y. V. Milman, in *Mechanical Properties and Deformation Behavior of Materials Having Ultra-Fine Microstructures*, edited by M. Nastasi, D. M. Parkin, and H. Gleiter. (NATO ASI Series E 233, 1993) pp. 605-610.
4. D. J. Lloyd, Int. Mater. Rev. **39**, 1 (1994).
5. M. F. Ashby, Philos. Mag. **21**, 399 (1970).
6. E. C. Eringen, *Microcontinuum Field Theories* (Springer, New York, 1999).
7. . A. Fleck and J. W. Hutchinson, J. Mech. Phys. Solids **41**, 1825 (1993).
8. J.Y. Shu and N.A. Fleck, J. Mech. Phys. Solids **47**(2), 297 (1999).
9. A. Acharya and J. Bassani, in *Micromechanics of Plasticity and Damage of Multiphase Materials*, IUTAM Symposium, Paris. Aug. 29 - Sept 1, 1995.
10. A. Wikström, Report **261**, Department of Solid Mechanics, Royal Institute of Technology, Stockholm, Sweden, 2000.
11. S. Sun, B.L. Adams, C. Shet, S. Saigal, and W. King, Scripta Met. **39**, 501 (1994).
12. M. M. Barney, G. H. Campbell, J. S. Stölken, J. M. Plitzko, W. E. King, and J.W. Morris, Multiscale Modeling of Materials, Editors: L.P. Kubin, J.L. Bassani, K. Cho, H. Gao, R.L.B. Selinger, MRS Proceedings Volume 653, Materials Research Society, Warrendale, PA, 2001.
13. W. E. King, G.H. Campbell, A.W. Coombs, G.W. Johnson, B.E. Kelly, T.C. Reitz, S.L. Stoner, W.L. Wien, and D.M. Wilson, in *Joining and Adhesion of Advanced Inorganic Materials*, edited by A. H. Carim, D. S. Schwartz and R. S. Silberglitt (Mat. Res. Soc. Symp. Proc. **314**, Pittsburgh, PA, 1993) p. 61.
14. A.A.MacDowell, R.S.Celestre, N.Tamura, R.Spolenak, B.C. Valek, W.L.Brown, J.C.Bravman, H.A.Padmore, B.W.Batterman & J.R.Patel, Nuclear Instruments and Methods in Physics Research A **467-468**, 936 (2001).

This work performed under the auspices of the Division of Materials Science of the Office of Basic Energy Sciences, U.S. Department of Energy, and the University of California Lawrence Livermore National Laboratory under contract No. W-7405-Eng-48.

Principal investigator: Robert O. Ritchie, Ernest Orlando Lawrence Berkeley National Laboratory. Email: roritchie@lbl.gov. Telephone: 510-486-5798.

# High Resolution Study of the Thermomechanical Behavior of Al(0.5wt% Cu) Thin Films by Scanning X-Ray Microdiffraction (μSXRD)

N. Tamura[1], B.C. Valek[3], R. Spolenak[2], R.S. Celestre[1], A.A. MacDowell[1], H.A. Padmore[1], B.W. Batterman[1,4] and J.R. Patel[1,4]

[1]Advanced Light Source, Ernest Orlando Lawrence Berkeley National Laboratory, University of California, Berkeley, California 94720, USA

[2]Agere Systems, formerly Bell Laboratories, Lucent Technologies, Murray Hill NJ 07974

[3]Dept. Materials Science & Engineering, Stanford University, Stanford CA 94305

[4]SSRL/SLAC, Stanford University, P.O. Box 43459, Stanford CA 94309, USA

## INTRODUCTION

Materials properties such as strength, resistance to fatigue, and failure ultimately depend on the microstructural features of the material, such as grains, grain boundaries, inclusions, voids and other defects. The so-called mesoscopic length scale (approximately between 0.1 and 10 μm) is receiving increasing attention, both theoretically and experimentally, in order to understand the mechanical behavior of polycrystalline samples as they experienced various constraints. Compared to single crystals, polycrystals are a highly inhomogeneous medium where local stress and structure variations are likely to play an important role in the overall macroscopic behavior of the material. In the present study, we are applying the Scanning X-Ray Microdiffraction (μSXRD) technique developed at the ALS [1,2] to probe local strain/stress and grain orientation in Al(0.5wt% Cu) thin films and compare the results with those obtained with conventional averaging techniques such as wafer curvature.

## EXPERIMENTAL

The samples investigated are sputtered Al (0.5 wt.% Cu) thin film test structures originally designed for electromigration studies. The patterned lines, passivated with 0.7 μm of $SiO_2$ (PETEOS), have dimensions 0.7 or 4.1 μm in width, 30 μm in length and 0.75 μm in thickness. Ti shunt layers are present at the bottom and the top of the lines. A 100 x 100 μm bond pad on the chip with a thin Ti underlayer is used to simulate a bare blanket film.

The samples were scanned under a submicron size white X-ray beam and at each step a white beam Laue diffraction pattern in reflective geometry was collected. The patterns were analyzed in order to yield the orientation and deviatoric strain/stress tensor under each illuminated points of the samples. The outputs of the analysis are grain orientation and strain/stress maps.

The bond pad (blanket film) was thermally cycled between 25°C and 345°C in 40° steps. At each temperature increment, a 15x15 μm area of the film was scanned with the focused white x-ray beam in 1 μm steps. A 0.7 μm wide line and 4.1 μm wide line were scanned in 0.5 μm intervals at room temperature. In addition, a 0.7 μm line was mapped in 0.5 μm steps across the line and 1 μm steps along the line at several temperatures during a cycle between 25°C and 305°C.

## RESULTS

A 5x5 μm area preliminary scan of the blanket film shows that while the film is (111) textured within 3°, the deviatoric stresses $\sigma_{xx}' \neq \sigma_{yy}'$ (In the x,y,z orthogonal coordinate system, z is the

out-of-plane direction). In particular, at the granular and subgranular level, the stress can depart significantly from biaxiality. However, if we average the data over the 5 × 5 μm scanned area, biaxiality is retrieved, i.e.: $\langle\sigma'_{xx}\rangle \approx \langle\sigma'_{yy}\rangle$. The average biaxial stress of the film can be computed assuming that the out-of-plane average total stress $\langle\sigma_{zz}\rangle = 0$. Expressing the total average stress matrix as the sum of the deviatoric and hydrostatic stress components one can show that the average biaxial stress $\langle\sigma_b\rangle = \langle\sigma_{xx}\rangle = \langle\sigma_{yy}\rangle = \langle\{(\sigma'_{xx}+\sigma'_{yy})/2\} - \sigma'_{zz}\rangle$.

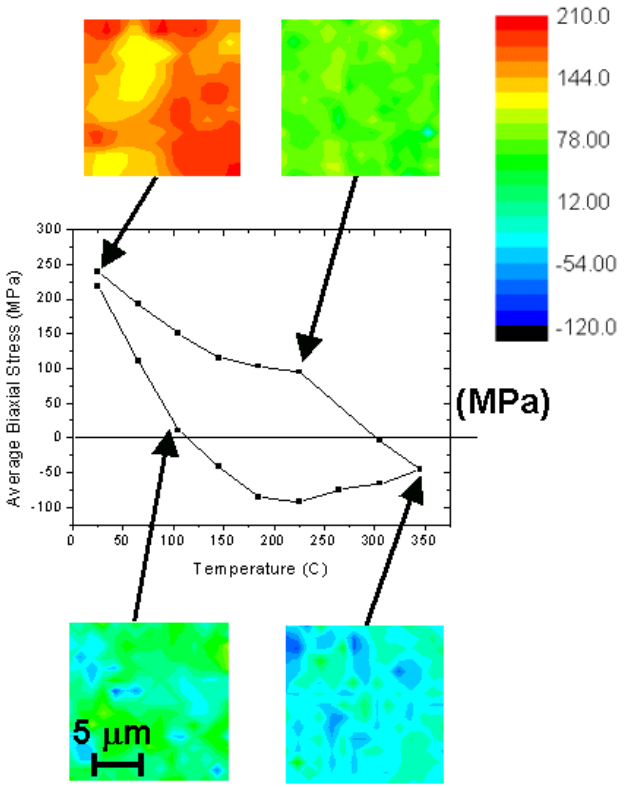


Figure 1. Thermal cycling results on a 15×15 μm area of an Al(Cu) bond pad (blanket film) showing the averaged biaxial stress component $\langle\sigma_b\rangle$ versus temperature. The insets show detailed stress distribution in the film at different temperatures (The 2D maps are a plot of $-\sigma'_{zz} = \sigma'_{xx} + \sigma'_{yy}$ as a measure of the in-plane stress). Note the blue regions of compressive stress in the 105 ºC map, while on average the stress is still in the tensile regime.

A plot of the average biaxial stress in the blanket film obtained by x-ray microdiffraction during a thermal cycle between 25°C and 345°C is shown in Fig. 1. The stresses in approximately 130 grains in a 15μm x 15μm region were averaged to give the results shown in the figure. Though our temperature range is about 100°C smaller, the temperature cycling curve using microdiffraction is very similar to that reported by Venkatraman et al [3] using wafer curvature measurements on an Al(Cu) films with thickness 1 μm. The film is in tension at room temperature, with an average biaxial stress of 230 MPa. The measured stress is caused by mismatch between the thermal expansion coefficients of the aluminum and the silicon substrate. Upon heating, the higher thermal expansion coefficient of the aluminum film relaxes the tensile stress before driving the film into compression. From Fig. 1 the experimentally determined initial thermoelastic slope is $(d\sigma / dT) = 2.53$ MPa / °C. The theoretical thermoelastic slope was calculated to be 2.34 MPa / °C, in reasonable agreement with the experimental value.

The real advantage of using μSXRD is however the possibility to obtain orientation and strain/stress information at a very local level, allowing for the study of mechanical properties of thin films with new visibilities. For instance, it provides a simple and straightforward explanation to the early departure from linearity of the thermoelastic slope during heating (seen in [3] as well as in the present data), even before the film enters in the compressive state. At room temperature, the stress is highly inhomogeneous with regions sustaining more tensile stress than others. Upon

heating some regions of the film become compressive while the average biaxial stress is still in the tensile regime. Even though the average stress is zero at about 100$^{o}$C some grains have already reached their yield stress and deformed and the heating curve departs from linearity. The temperature at which the curve departs from linearity is quite variable for different films and depends on detailed process parameters.
Similar local variations of the stress are observed in the passivated lines. These local variations increase with decreasing line width while the area of the hysterisis of the stress-temperature curves decreased. The hysteresis area is typically a measure of the amount of plastic deformation experienced by the material. In the case of submicron sized lines, the passivation layers introduce additional constraints to the dislocation motions, as compared to the case of unpassivated blanket films [4]. These local stress variations which do not always follow grain boundaries but can be intragranular, are quite surprising in an elastically isotropic material as aluminum. However these differences can be explained by differences in grain sizes and grain-to-grain interactions [5].

## ACKNOWLEDGMENTS

The authors thank Intel Corp. for the partial funding of the end station.

## REFERENCES

1. A. A. MacDowell, R. S. Celestre, N. Tamura, R. Spolenak, B. Valek, W. L. Brown, J. C. Bravman, H. A. Padmore, B. W. Batterman, and J. R. Patel, Nucl. Instr. & Meth. In Phys. Res. **A 467-468**, 936 (2001).
2. N. Tamura, R. Spolenak, B.C. Valek, A. Manceau, N. Meier Chang, R.S. Celestre, A.A. MacDowell, H.A. Padmore and J.R. Patel, Rev. of Sci. Instr., **73** (2002) in press.
3. R. Venkatraman, J. C. Bravman, W. D. Nix, P. W. Davies, P. A. Flinn, D. B. Fraser. J. of Electron. Matls. **19**, 1231 (1990).
4. B.C. Valek, N. Tamura, R. Spolenak, A.A. MacDowell, R.S. Celestre, H.A. Padmore, J.C. Bravman, W.L. Brown, B. W. Batterman and J. R. Patel, Mat. Res. Soc. Symp. Proc., **673**, P.7.7.1 (2001).
5. R. Spolenak et al. (2002) this compendium.

This work was supported by the Director, Office of Science, Office of Basic Energy Sciences, Materials Sciences Division, of the US Department of Energy under Contract No. DE-AC03-76SF00098 at Lawrence Berkeley National Laboratory.

Principal investigator: Nobumichi Tamura, Advanced Light Source, Ernest Orlando Lawrence Berkeley National Laboratory. Email: NTamura@lbl.gov. Telephone: 510-486-6189.

# In-situ Synchrotron X-ray Microdiffraction Study of Deformation Behavior in Copper-Polycrystals during Uniaxial Deformations

H.D. Joo[1], J.S. Kim[1], K. H. Kim[1] , N. Tamura[2], and Y. M. Koo[1]
[1] *Center for Advanced Aerospace Materials, Dept. Materials Science & Engineering, Pohang University of Science and Technology, Pohang 790-784, South Korea*
[2] Lawrence Berkeley National Laboratory, University of California, Cyclotron Road, Berkeley, CA94720, USA

## INTRODUCTION

Recent experiments have shown that the plastic deformation and the fracture of solid have relation with the formation of dislocation cell structure and the rotation of structural elements[1]. Therefore, attention should be focused on a mesovolume of deformed material. Because The local stress and strain differ from those averaged at the macroscale, the discrete nature of the micro-deformation of the mesofragments should be accounted for the rotation of the different mesofragments being parts of subgrain, a grain, grains, etc., which plays an important role in plasticity. Moreover, In-situ study of deformation behavior in polycrystalline material during deformations at microlevel had not been performed. In the present work, we have investigated plastic deformation behavior in polycrystalline material during deformations at microlevel using the X-ray Microdiffraction technique on beamline 7.3.3. at the ALS. This technique allows the measurements of local orientation and strain in microvolume element within a grain. In addition, an accuracy of this technique is about $2x10^{-4}$ in strain and less than $0.01^{o}$ in orientation[2].

## EXPERIMENT

The material used in the present study was a 99.999% pure polycrystal of copper. A tensile sample, with a gauge length of 7.5mm and a cross-section of 2x0.5 mm, was prepared by spark-erosion cutting. After mechanical polishing, the sample was annealed in a vacuum at 600□ for 30min. and chemically polished to remove damaged and oxidized surface material formed during mechanical polishing and heat treatment.

The synchrotron radiation source of beam line 7.3.3 at the Advanced Light Source (ALS) was used for the *in situ* Microdiffraction Laue experiment, described in [2,3]. In order to measure Orientation and strain/stress distributions at each strain(0, 2, 4, 6, 8, 10, 15, 20, 25, 30% strain), a large number of diffraction pattern are collected by scanning the sample and analyzed. The beam size of experiment was 1.5μm x 1.5μm and the detector was a charge-coupled device camera. The samples were elongated in steps of 0.15 mm by a tensile device mounted on the translation stage. The strain rate was $2.22x10^{-4}$ .

## RESULTS AND DISCUSSION

Figure 1 shows the orientation distribution of Copper sample at each deformation step(0, 2, 4, 6% strain). The tensile direction is vertical in the plots. The orientation of big center grain starts to change starting in the middle of the grain as the tension applied. In order to consider the heterogeneities of the deformation-induced microstructure within single grains, tensile axis rotation in other position within a grain is measured. We take five local positions in center grain which are Ag, Bg, Cg, Dg and Eg position, and measure the tensile axis rotation at each point. Figure 2(a) shows positions of 5 points.

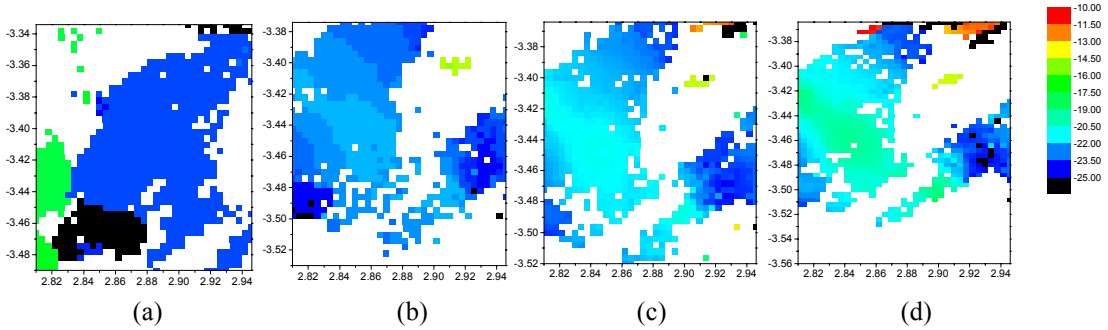


Fig.1.Grain Orientaion distribution of Copper sample at each deformation step((a)0, (b) 2, (c) 4, (d) 6% strain).

Figure 2(b)(c) shows rotation angle from initial position as a function of strain at each strain, and the orientation of neighbor grains in standard triangle, respectively. The tensile axis rotation at Ag position is larger than that at Dg position. The initial orientation of grain 2,8 near Ag position is similar to that of center grain while the angle between grain 5,6 and center grain is quite large. That is, the grain boundary in diagonal direction is small angle boundary. In the orientation map, primary slip direction ($\bar{1}01$) at sample coordination is (0.172,-0.363, 0.378) which is a diagonal direction in the plot. This phenomenon may be due to differences in the selection of simultaneously acting slip systems among neighboring volume elements of individual grains and different part of grain interior. Lattice rotation near high angle grain boundary is large while Lattice rotation near low angle grain boundary is small. This means that Grain boundary and grain orientation affect the slip behavior.

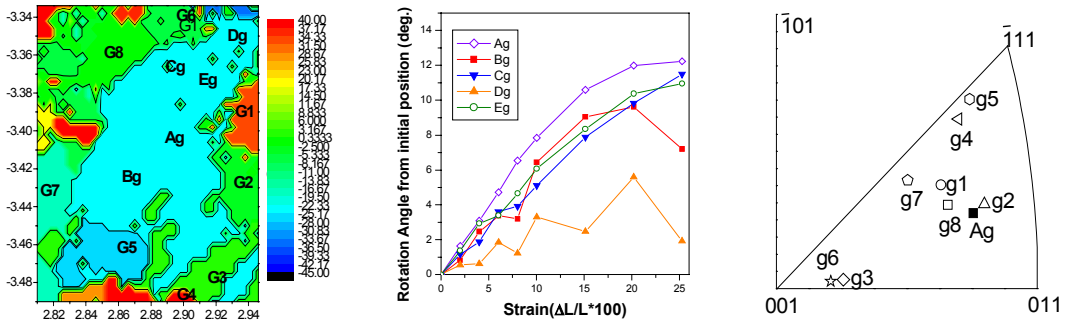


Fig.2. (a) shows positions of 5 points,(b)(c) shows rotation angle from initial position as a function of strain at each strain, and the orientation of neighbor grains in standard triangle, respectively.

## REFERENCES

1. N.Hansen, Mater. Sci. Engng. **6**, 1039 (1990).
2. A. A. MacDowell, R. S. Celestre, N. Tamura, R. Spolenak, B. Valek, W. L. Brown, J. C. Bravman, H. A. Padmore, B. W. Batterman and J. R. Patel, Nuclear inst. Meth. **467-468**, 936 (2001).
3. N. Tamura, R. Spolenak, B.C. Valek, R.S. Celestre, A.A. MacDowell, H.A. Padmore and J.R. Patel, **"**Orientation and Stress Mapping on Beamline 7.3.3.: a New Tool to Study Material Properties at Submicron Scale", ALS activity report 2000.

This work was supported by POSTECH (Pohang University of Science and Technology) and materials analysis team of RIST(Research Institute of Industrial Science & Technology)

Principle investigator: H.D. Joo, Center for Advanced Aerospace Materials, Pohang University of Science and Technology, e-mail:matter@postech.ac.kr, Telephone: 82-54-279-5130.

# Local Plasticity in Al(0.5wt% Cu) Membranes Revealed by Scanning X-Ray Microdiffraction (μSXRD)

R. Spolenak[2], N. Tamura[1], B.C. Valek[3], R.S. Celestre[1], A.A. MacDowell[1], H.A. Padmore[1], W.L. Brown[2], B.W. Batterman[1,4] and J.R. Patel[1,4]

[1]Advanced Light Source, Ernest Orlando Lawrence Berkeley National Laboratory, University of California, Berkeley, California 94720, USA

[2]Agere Systems, formerly Bell Laboratories, Lucent Technologies, Murray Hill NJ 07974

[3]Dept. Materials Science & Engineering, Stanford University, Stanford CA 94305

[4]SSRL/SLAC, Stanford University, P.O. Box 43459, Stanford CA 94309, USA

## INTRODUCTION

While polycrystalline materials are ubiquitous in the industry of metal thin films, the understanding of polycrystal plasticity still constitutes a theoretical challenge. The problem arises from the fact that grain boundaries introduce a factor of complexity in plastic deformation that can not be adequately studied by conventional averaging techniques. On the other hand, transmission electron microscopy techniques, besides probing too fine a length scale to be statistically significant, cannot usually measure strain/stress of the material without disturbing its initial state (thinning). We have shown that the white beam μSXRD technique [1,2], developed at the ALS on beamline 7.3.3. is capable of measuring orientation and strain/stress variations in the correct mesoscale length scale without the need of any sample preparation which can alter the microstructure or true stress state of the material under investigation. In one of our study [3], we showed significant inter- as well as intragranular stress variations in polycrystalline Al thin films sputter deposited on a silicon wafer, in apparent contradiction with the nearly isotropically elastic properties of aluminum. The present study on a thin Al membrane, shows that grain-to-grain interactions play a prominent role in the understanding of the local stress distribution and must be considered as key parameters in the modeling of polycrystal plasticity.

## EXPERIMENTAL

The sample is a Al(0.5 wt.% Cu) film deposited at 400 °C on a 200 nm thick $SiN_x$ membrane on a Si frame and is used for in-situ bulge test experiment [4] allowing to apply stress to the film by differential pressure bulging. The aspect ratio of 1:6 of the membrane ensures a macroscopically uniaxial stress across the narrow dimension of the film.
μSXRD data were collected by scanning the same 15x15 μm area of the film while differential pressure ranging from 0 to 250 Torrs were applied. At each step of the scans (step size of 0.5 μm), a white beam Laue pattern was collected, from which grain orientation and deviatoric stress tensor is deduced [1,2].

## RESULTS

Even before applying any differential pressure, the residual stress in the film appears in our μSXRD experiments to be strongly non-inhomogeneous with local variations reaching 100 MPa. The variations are both inter and intragranular. In particular shear stresses at grain boundaries can be significant. The stress state at room temperature is primarily a result of cool down from the 400 °C deposition temperature due to the difference in thermal expansion coefficients between

the film and the substrate. A wide distribution in stress implies a wide distribution in yield stresses, and can be explained by a grain size effect. Dislocation motions are limited by grain boundaries and the yield stress is on average inversely proportional to the grain size [5]. However a distribution of yield stresses due to difference in grain size or orientation cannot solely account for all aspects of the stress distribution. Our data indicate that the actual stress in the film is the result of complex interactions between different grains while experiencing a macroscopic applied stress. In particular, the stress state of a given grain is strongly influenced by those of its immediate neighbors as schematized in Fig. 1. A high yield stress area (small grains) and a low yield stress area (big grains) are sandwiched between two boundary grains. When an external constraint is applied, a shear stress appears at the boundary between the two different yield stress areas and a stress gradient appears in the boundary grains.

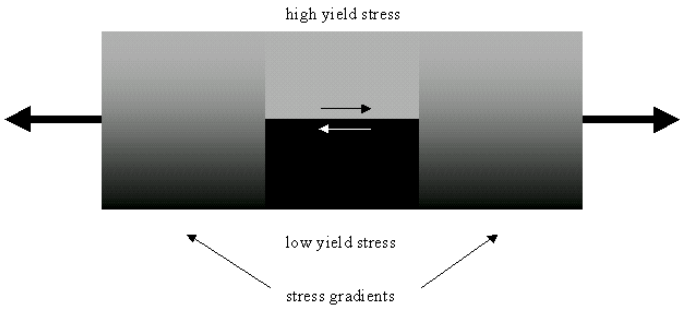


Fig. 1.- Schematic behavior of two grains with two different yield stresses sandwiched between two boundaries grains as an external force is applied.

Both effects are observed in the experimental data (Fig. 2). Grain B act as a high yield stress grain while grain C has a low yield stress. Shear stress is observed at the boundary between grain B and C (see $\sigma_{xy}$ distribution) while a bottom to top stress gradient is evident in grain A (see $\sigma'_{xx}$ and $\sigma'_{zz}$ distributions).

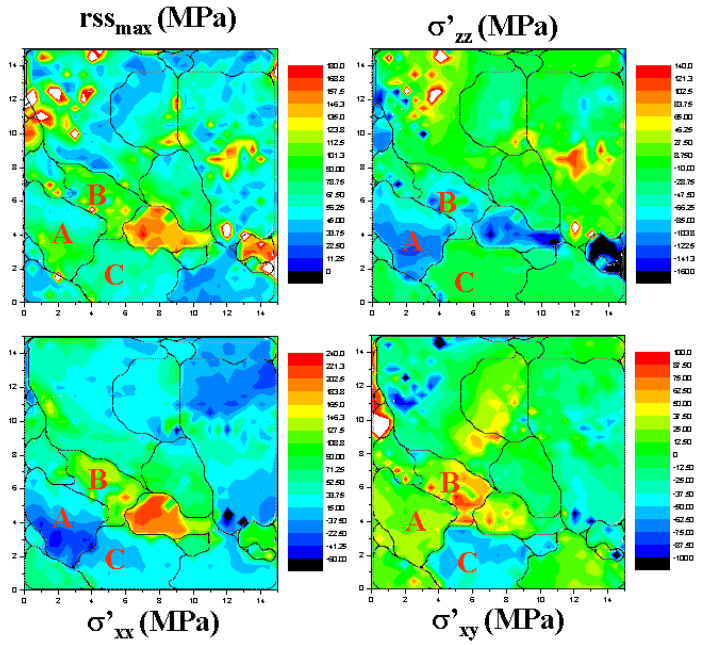


Fig. 2.- Resolved shear stress, deviatoric stress and shear stress as measured by μSXRD on an Al membrane under stress.

The active glide system in a given grain can be inferred by using the maximum resolved shear stress criterion (which is calculated from the deviatoric stresses considering the 12 {111}/<110>glide systems for fcc crystals). Our in-situ bulge test experiment clearly shows

changes in the active glide systems while the film experiences increasing applied stress during the in-situ bulge test experiment. In particular we notice that changes in the glide system can occur in part of a given grain under the influence of the changing stress state and shape of the neighboring grains. Therefore, during plastic deformation in polycrystals, large grains behave more like a collection of small grains (subgrains) rather than single crystals. This concept of an effective grain size where the material deforms uniformly, and which can be smaller than the physical grain size, is a direct consequence of the grain-to-grain interactions during deformation.

## ACKNOWLEDGMENTS

The authors thank Intel Corp. for the partial funding of the end station.

## REFERENCES

1. A. A. MacDowell, R. S. Celestre, N. Tamura, R. Spolenak, B. Valek, W. L. Brown, J. C. Bravman, H. A. Padmore, B. W. Batterman, and J. R. Patel, Nucl. Instr. & Meth. In Phys. Res. **A 467-468**, 936 (2001).
2. N. Tamura, R. Spolenak, B.C. Valek, A. Manceau, N. Meier Chang, R.S. Celestre, A.A. MacDowell, H.A. Padmore and J.R. Patel, Rev. of Sci. Instr., **73** (2002) in press.
3. B.C. Valek, N. Tamura, R. Spolenak, A.A. MacDowell, R.S. Celestre, H.A. Padmore, J.C. Bravman, W.L. Brown, B. W. Batterman and J. R. Patel, Mat. Res. Soc. Symp. Proc., **673**, P.7.7.1 (2001).
4. R. Spolenak, C. A.Volkert, S. Ziegler, C. Panofen and W.L. Brown, Mat. Res. Soc. Symp. Proc., **673**, P.1.4.1 (2001).
5. R. Venkatraman and J.C. Bravman, J. Mater. Res. **7**, 2040 (1992); C. V. Thompson, J. Mater. Res. **8** (2), 237-238 (1993)

This work was supported by the Director, Office of Science, Office of Basic Energy Sciences, Materials Sciences Division, of the US Department of Energy under Contract No. DE-AC03-76SF00098 at Lawrence Berkeley National Laboratory.

Principal investigator: Nobumichi Tamura, Advanced Light Source, Ernest Orlando Lawrence Berkeley National Laboratory. Email: NTamura@lbl.gov. Telephone: 510-486-6189.

# MACRO STRESS MAPPING ON THIN FILM BUCKLING

P. Goudeau[1], P. Villain[1], N. Tamura[2], R.S. Celestre[2] and H. Padmore[2]
[1]Laboratoire de Métallurgie Physique, UMR 6630 CNRS, Université de Poitiers, SP2MI, Téléport 2, Bd M. et P. Curie, BP 30179, 86962 Futuroscope Chasseneuil cedex, FRANCE
[2]Advanced Light Source, LBNL, 1 Cyclotron Road, MS 2-400, Berkeley, CA, 94270, USA

## INTRODUCTION

Thin films deposited by Physical Vapor Deposition techniques on substrates generally exhibit large residual stresses which may be responsible of spontaneous detachment of the film from the substrate (stress relaxation) and in the case of compressive stresses, thin film buckling. Although these effects are undesirable for future applications, one may take benefit of it for thin film mechanical properties investigation [1-4]. Since the 80's, a lot of theoretical works have been done to develop mechanical models and calculations (elasticity of thin plates, fracture mechanic) with the aim to get a better understanding of driven mechanisms giving rise to this phenomenon and thus to propose solutions to avoid such problems. Nevertheless, only a few experimental works have been done on this subject to support these theoretical results and nothing concerning local stress/strain measurement mainly because of the small dimension of the buckling (fig. 1). In this experiment, we propose to use micro beam x-ray diffraction available on synchrotron radiation sources as a local probe (spatial) for stress/strain analysis of thin film buckling. The main objectives are to apply x-ray micro beam diffraction in first for determining macro residual stresses at the top of the buckle (comparison with adherent region on the film) in different systems (W, Mo, Au on silicon) and in a second step for scanning the buckling with the smallest x-ray beam size in order to realize macro stress mapping.

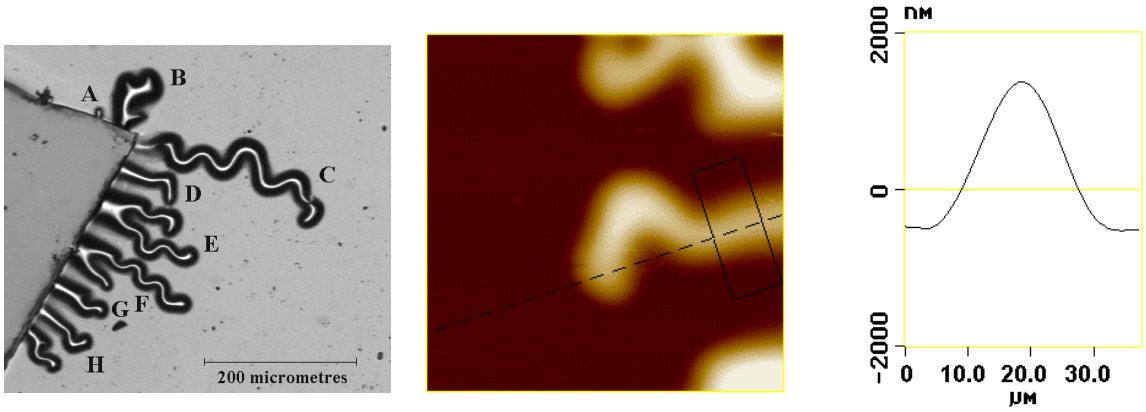


(a) (b) (c)

**Figure 1** : *Wrinkles observed by optical microscopy (a) close to a step realised during the deposition process for film thickness measurement and AFM images (b) of buckling noted D on (a) and corresponding cross section, (c) perpendicular to the propagation direction.*

## EXPERIMENTAL METHOD

Among the most widely used method to determine the stress level in thin films, x-ray diffraction (XRD) is phase selective and the unique non destructive technique which allows to determine both the mechanical and microstructural state of the diffracting phases. Indeed, the distance between atomic planes is used as an internal strain gauge. For polycrystalline samples, the

measurement of the diffraction peak position shift using $\sin^2\psi$ method allows to extract the stress tensor and the stress free lattice parameter [5]. However, x-ray diffraction is difficult to use in low dimensional systems because the diffracted intensities are weak due to the reduced thicknesses and nanocrystalline character of such materials. These problems may be solved using intense x-ray sources such as synchrotron radiation (S.R.). In addition to the high flux characteristic of S.R. facilities, the wide wavelength spectra and the optics (micro beam) which are available on beam lines ($3^{rd}$ generation SR only) allow to perform specific XRD experiments which are not possible with classical x-ray sources in laboratories.

The 7.3.3.1 Microdiffraction beam line at ALS provides a reduced spot size less than 1 $\mu m^2$ (Kirkpatrick Baez mirrors) with high flux for white or monochromatic radiation (4-crystals channel cut monochromator: 6-14 KeV). These performances are unique and perfectly adapted to our project [6]. In our samples, the grain size ( $\leq$ 10 nm) is smaller than the x-ray beam one and macro-strains are of about 0.5-1 %. The diffraction pattern recorded with a 2D CCD detector is composed of different rings which allow to extract (using specific software - to be developed) the in-plane stress without any tilt of the samples (the $\psi$ *description* is contained in the 2D pattern and the angular resolution is enough to appreciate such large macro-strains). Accurate spatial spot localization on the sample surface is achieved from markers delimiting the region of interest. A precise goniometer allows XRD measurements in reflection mode and an X-Y translation stage is used for scanning the sample surface.

## FEASIBILITY OF THE EXPERIMENT

Preliminary microdiffraction experiments have been successfully done in June 2001. 630 nm thick gold films deposited on silicon (100) substrates covered with native oxide have been chosen for these measurements. The delamination of the thin film is evidenced on figure 2 (a) and an individual buckle is shown on figure 2 (b); its shape corresponds to a portion of a sphere. The position of the buckle (x,y) is determined from the step corner coordinates (x0,y0) which have been measured by X-ray fluorescence (white beam). This step has been realized during the film deposition.

The calibration of the 2D diffraction diagram is done from the diffraction of the single crystal silicon substrate using white x-ray beam. The diffraction pattern obtained in an adherent (flat) region of the gold film is shown on figure 3. Because of the <111> texture of the film, we observe maximum intensities on each two rings for particular pole directions X. During the scan of the buckle A with a 10 $\mu m$ step , the position of the two maximum intensities (X+ and X-) moves along the ring because of the rotation of the normal to the film surface around x and y axis. Thus, from the diffraction pattern, one may deduce the position of the beam on the buckle and the corresponding strains in this region. A comparison between the diffraction diagrams obtained in flat regions and at the top of the buckle indicates a stress relaxation.

A complete interpretation of the data is still under progress because specific tools and methodologies have to be applied for diffraction pattern analysis. Accuracy and sensibility are the two main points to be considered for strain variation during the scan. Furthermore, Finite Element calculations have been engaged for such spherical gold buckles. Further experiments will concern not only metallic thin films but also structural biomaterials such as diamond coatings on Titanium based alloys (TA6V) which are promising candidates for medical

prostheses. Our laboratory is engaged in a French government program called A.C.I. with two other French laboratories. It concerns in particular, the influence of residual stresses (about –5 GPa in C-diam) on the mechanical behavior of such systems.

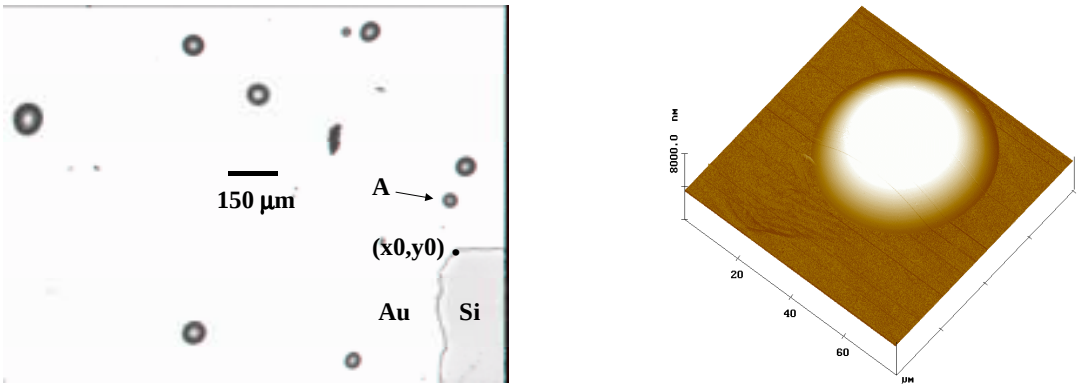


(a) (b)

**Figure 2.** *630 nm gold film sputter deposited on Si substrate: (a) optical image of the sample surface and (b) AFM image of the buckle noted A on fig. (a); the in plane width is around 40 µm and the height of 1.2 µm.*

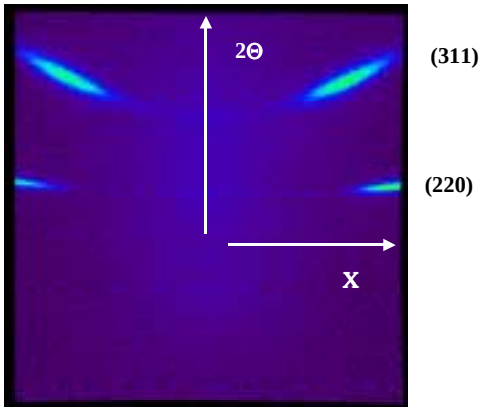


**Figure 3:** *2D X-ray diffraction diagram obtained on an adherent gold film region with an X-ray energy of 5.7 keV, a spot size on the sample of 3 x 3 µm$^2$ and a recording time of 300 sec.*

## REFERENCES


1. M. Talea, B. Boubeker, F. Cleymand, C. Coupeau, J. Grilhé, P. Goudeau, Mat. Let. **41**, 181 (1999).
2. C. Coupeau, J.-F. Naud, F. Cleymand, P. Goudeau, J. Grilhé, Thin. Sol. Films **353**, 194 (1999).
3. V. Branger, C. Coupeau, P. Goudeau, B. Boubeker, K.F. Badawi, J. Grilhé, J. of Mat. Sci. Let. **19**, 353 (2000).
4. B. Boubeker, M. Talea, Ph. Goudeau, C. Coupeau, J. Grilhé, Mat. Charac. **45**, 33-37 (2000).
5. V. Branger, V. Pelosin, P. Goudeau, K.F. Badawi, High Temp. Mat. Proc. **2**, 419-429 (1998).
6. P. Goudeau in *Photomechanics 2001*, edited by Y. Berthaud et al.(GAMAC, France), 87-94.



This work was initiated with support of the Advanced Light Source at the Lawrence Berkeley National Laboratory.



Principal investigator: Philippe Goudeau, Laboratoire de Métallurgie Physique – UMR 6630 CNRS – Université de Poitiers, France. Email : Philippe.Goudeau@univ-poitiers.fr. Telephone : 33 5 49 49 67 26. Fax : 33 5 49 49 66 92

# Microstructure and pinning properties of hexagonal-disc shaped single crystalline $MgB_2$

C. U. Jung[1], J. Y. Kim[1], P. Chowdhury[1], Kijoon H. P. Kim[1], Sung-Ik Lee[1], N. Tamura[2], W. A. Caldwell[2], and J. R. Patel [2,3]

[1]National Creative Research Initiative Center for Superconductivity and Department of Physics, Pohang University of Science and Technology, Pohang 790-784, Republic of Korea

[2]Lawrence Berkeley National Laboratory, Advanced Light Source, 1 Cyclotron Road, MS-2-400 Berkeley, CA 94720, USA

[3] SSRL/SLAC, Stanford University, CA 94309, USA

## INTRODUCTION

The existence of impurities and structural imperfections on a microscopic scale can result in diverse transport and pinning properties in $MgB_2$, which was even observed for single crystalline samples made by several groups[1-3]. Here, we report the X-ray micro-diffraction measurements for, $MgB_2$ single crystals with hexagonal-disc shapes and shiny surfaces. The diagonal length and the thickness for the largest crystal was about 100 μm and 10 μm, respectively. The crystallinity was thoroughly identified by using the Laue pattern in the X-ray micro-diffraction measurement. Both the edge and the c-axis of the hexagonally shape disc were found to match the crystal symmetry.

## EXPERIMENTAL

Two different procedures were used to grow the single crystals, and in both cases, excess Mg was critical for the growth of single crystals. The first involved a two-step method in which already synthesized pieces of $MgB_2$ bulk[4] were used as a seed material. They were heat treated in a Mg flux inside a Nb tube, which was sealed in an inert gas atmosphere. Then, the Nb tube was put inside a quartz tube, which was sealed in vacuum. The quartz tube was heated for one hour at 1050 °C, cooled very slowly to 700 °C for five to fifteen days, and then quenched to room temperature. The crystal images were observed using a polarizing optical microscope and a field-emission scanning electron microscope (SEM). We successfully separated single-crystalline $MgB_2$ from the Mg flux by using a thermo-mechanical spinning method.

For the X-ray micro-diffraction measurements, several crystals were fixed at the center of Cu crosshairs on the substrate, as shown in Fig. 1. The instrument used at the Advanced Light Source (ALS) for X-ray micro-diffraction is capable of producing a submicron-size X-ray microbeam and with submicron spatial resolution can probe the local texture in a single crystal[5]. The sample was positioned using the Cu fluorescence signal detected from the Cu crosshairs on the Si substrate by using a high-purity Ge ORTEC solid-state detector connected to a multichannel analyzer. The crystal orientation with respect to the substrate can be determined with an accuracy of 0.01 degree.

## RESULTS

The crystal structure was identified by using white beam X-ray micro-diffraction measurements. After positioning these single crystals, a 100 μm × 100 μm region between the Cu crosshairs was scanned with a step size of 2 μm. At each step, the Laue pattern (together with the Cu *K*

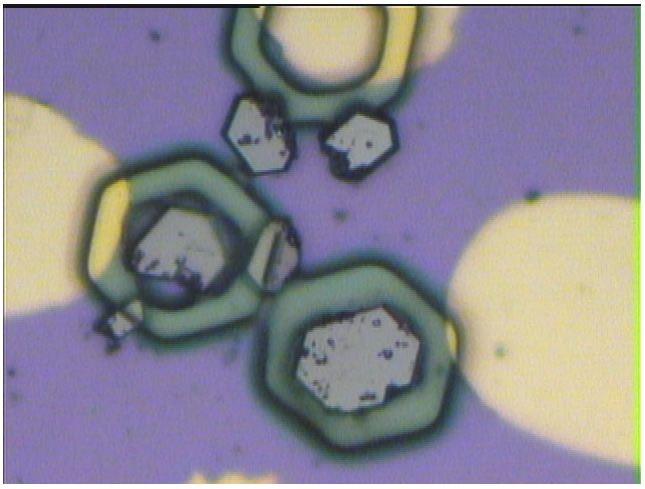

Figure 1. Polarizing optical microscope images of $MgB_2$ single crystals. An epoxy was used to fix six single crystals at the center of 100 μm-wide Cu crosshairs.

fluorescence signal ) was collected with a BRUKER 6000 CCD camera which has an active area of 9 × 9 cm and was placed about 4 cm above the sample. [2500 images, 1024 pixel ×1024 pixel mode] The exposure time at each step, was 1 second. An example of a Laue pattern obtained from a $MgB_2$ single crystal is shown in Fig. 2(a). The Laue patterns are consistent with a hexagonal $MgB_2$ structure (a =0.3086 nm, c = 0.3524 nm, Space Group number =191, Ref. 6). The (0005) reflection in the center of the pattern in Fig. 2(a) corresponds to the direction of the normal to the crystal surface. This confirms that the surface plane normal is along the c-axis. Moreover, the hexagonal edges of the crystals were found to match the <1,0,-1,0> directions within a fraction of a degree resolution. Thus, the shapes of the crystals in the microscope image followed the $MgB_2$ crystal symmetry, which will be quite useful for any research of the direction dependencies of the physical properties in $MgB_2$.

Indexing the Laue patterns in Fig. 2(a) allowed us to calculate the complete orientation matrix of the X-ray illuminated volume. A finer step size of 1 μm was used for the white-beam scan. The orientation variations inside the single crystal shown in the right bottom corner of Fig. 1 are shown in Figs. 2(b) and 2(c). Figure 2(b) is the out-of-plane orientation variation calculated as the angle between the c-axis and the normal to the surface of the silicon substrate. The out-of-plane variation was about 0.2 degrees between the light orange and the red regions. The out-of-plane orientation shows a variation of about 0.2 degrees between the bottom and the top parts, indicating a slight bending of the crystal (which might be due to the photoresist used as an epoxy). Figure 2(c) shows the in-plane orientation variation calculated as the angle between the measured a-axis (or b-axis) and a reference directions. The variation was about 0.4 degrees between the light blue-green and the green regions. The in-plane orientation also showed some inhomogeneities of up to about 0.2 degrees.

These results demonstrate that the orientation of crystal axis of our hexagonal-disc-shaped single crystals was perfect, within 0.2 degrees[7]. A recent study showed that (0001) twist grain-boundaries, formed by rotations along the c-axis (typically by about 4 degrees), were the major grain boundaries in polycrystalline $MgB_2$ [8].

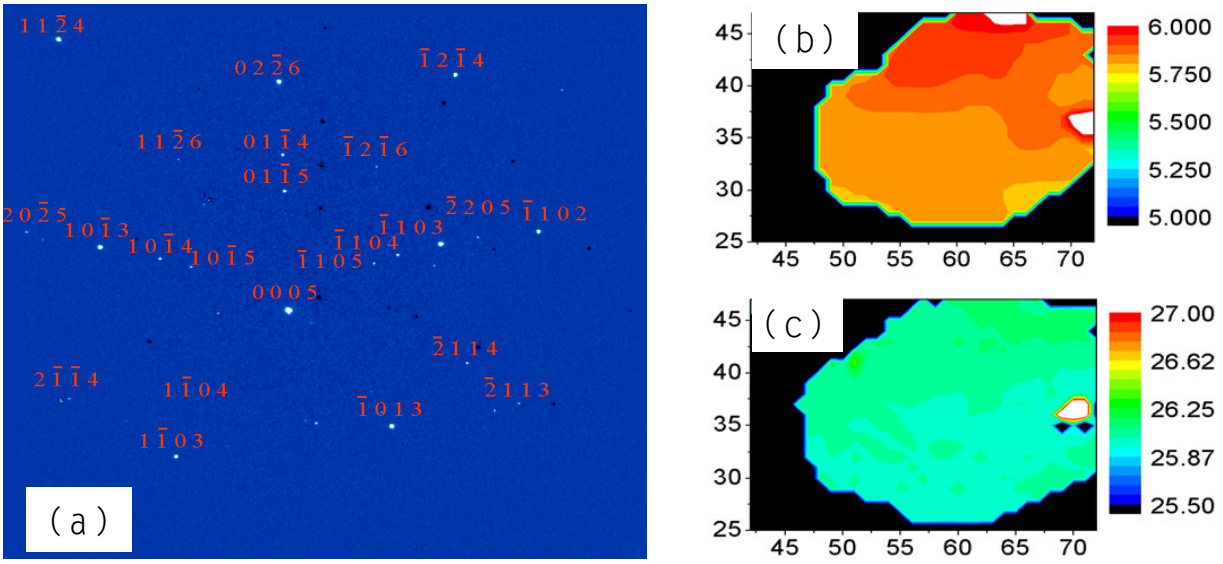


Figure 2. (a) A representative image of an indexed Laue pattern from X-ray micro-diffraction. (b) and (c) are, respectively, for the out-of-plane and the in-plane orientations inside a single crystal.

## REFERENCES


1. S. Lee, H. Mori, T. Masui, Yu. Eltsev, A.Yamamoto, and S.Tajima, J. Phys. Soc. Jpn. **70**, 2255 (2001).
2. M. Xu, H. Kitazawa, Y. Takano, J. Ye, K. Nishida, H. Abe, A. Matsushita, N. Tsujii, and G. Kido, Appl. Phys. Lett. **79**, 2779 (2001).
3. O. F. de Lima, R. A. Ribeiro, M. A. Avila, C. A. Cardoso, and A. A. Coelho, Phys. Rev. Lett. **86**, 5974 (2001).
4. C. U. Jung, Min-Seok Park, W. N. Kang, Mun-Seog Kim, Kijoon H. P. Kim, S. Y. Lee, and Sung-Ik Lee, Appl. Phys. Lett. **78**, 4157 (2001)
5. A. A. MacDowell, R. S. Celestre, N. Tamura, R. Spolenak, B. C. Valek, W. L. Brown, J. C. Bravman, H. A. Padmore, B. W. Batterman, and J. R. Patel, Nucl. Instrum. Meth. A **467-468**, 936 (2001).
6. J. Nagamatsu, N. Nakagawa, T. Muranaka, Y. Zenitani, and J. Akimitsu, Nature **410**, 63 (2001).
7. C. U. Jung *et al*., to be submitted to Phys. Rev B.
8. Y. Zhu, L. Wu, V. Volkov, Q. Li, G. Gu, A. R. Moodenbaugh, M. Malac, M. Suenaga, and J. Tranquada, Physica C **356**, 239 (2001).



The work done at the Advanced Light Source is supported by the Director, Office of Science, Office of Basic Energy Sciences, Materials Sciences Division, of the U.S. Department of Energy under Contract No. DE-AC03-76SF00098 at Lawrence Berkeley National Laboratory. Part of work done at PSC is supported by the Ministry of Science and Technology of Korea through the Creative Research Initiative Program.



Principal investigator: Nobumichi Tamura, Advanced Light Source, Ernest Orlando Lawrence Berkeley National Laboratory. Email: ntamura@lbl.gov. Telephone: 510-486-6189.

# Monitoring anthropogenic metal released in the environment via X-ray fluorescence, absorption and diffraction at micrometer scales of resolution

A. Manceau[1,2], M.A. Marcus[1], N. Tamura[1], R.S. Celestre[1], A.A. MacDowell[1], R.E. Sublett[1], H.A. Padmore[1], M. Kersten[3]
[1]Advanced Light Source, Lawrence Berkeley National Laboratory, Berkeley, CA 94720
[2]Environmental Geochemistry Group, Hilgard Hall, University of California, Berkeley, CA 94720
[3]Geoscience Institute, Gutenberg University, 55099 Mainz, Germany

## INTRODUCTION

Ferromanganese nodules are common in aquatic systems, including lacustrine and shallow marine environments, and also on the oceanic seafloor. They generally have a banded structure consisting of practically pure and alternating Fe- and Mn-rich layers separated by mixed Fe-Mn zones. This concretic onion-like growth pattern is attributed to intermittent oxidizing and reducing conditions. Accretion of ferromanganese nodules may cover time scales up to millions of years. The implication that they provide a continuously growing substrate with constant sorption efficiency for trace elements is the basis of a resuming interest for Fe-Mn nodules focusing on their possible use as a paleoproxy record for long-term environmental changes. Therefore, an idea was born to try and assess the metal fluxes into the ferromanganese nodules by dating individual nodule growth layers, and to compare these fluxes with the temporal variability in anthropogenic emissions. The prerequisite for such an approach is high-resolution profiling due to the slow accretion of the nodule material. Synchrotron-based micro-X-ray fluorescence (μSXRF) was applied to obtain in-situ trace element profiles of the necessary spatial resolution, as a basis for the evaluation of nodule accretion rates and for an assessment of their use for retrospective monitoring of excess metal input in the western Baltic Sea. Then, in-situ X-ray diffraction (XRD) and extended X-ray absorption fine structure (EXAFS) spectroscopy at the Mn and Zn K-edge were performed at the micrometer resolution to determine how anthropogenic Zn is taken up.

## EXPERIMENTS

The examined nodule was collected in shallow water of the SW Baltic Sea where nodules are relatively fast-growing and enriched in metal contaminants, thus making them highly suitable to record the anthropogenic pollution in the last century. The sample was prepared as a micropolished 30 μm-thick thin section. The μXRD patterns of Fe- and Mn-pure layers were recorded on Beamline 7.3.3., and μEXAFS spectra were collected on Beamline 10.3.2. In both experiments, μSXRF maps were first recorded to image the Fe and Mn layers. All experiments were conducted with a beamsize of 15 (H) x 5 to 10 (V) μm.

## RESULTS AND INTERPRETATION

The μSXRF element map of Fe and Mn (Fig. 1) shows the typically cuspate zebra-type band structure of the Fe-Mn concretions. The thickness of Mn-rich layers varies typically from 200 to 500 μm and that of the Fe-rich layers from about 100 to 200 μm. Of the trace elements investigated (Co, Ni, Cu, and Zn), Zn showed the most significant enrichment, with values in the outermost surface Mn layers of up to six-fold higher than those found in older core parts. Thus, the high-resolution Zn profiles provide the necessary temporal resolution for a dating method

analogous to dendrochronology. Assuming a continuous accretion of these relatively fast growing nodules (on average 20 µm $yr^{-1}$) over the last century, the Zn enrichment was assessed to have commenced in 1880/90, reflecting the enhanced heavy metal emissions with rising industrialization in Europe. µXRD patterns collected in Fe-rich regions (Fig. 2) contain only a broad and faint double hump with maxima at about 2.85 Å and 2.25 Å. The centroid of this hump is at about 2.5 Å as in poorly-crystallized two-line ferrihydrite (hydrous ferric oxide). Minor amounts of detrital quartz grains and silica particles (opal-A) were also detected by µXRD. The µXRD patterns taken in the Mn-rich layers look completely different consisting of a series of basal reflection peaks at 7.07 Å (001), 3.51 Å (002) and *hk*0 peaks at 2.46 Å (200) and 1.43 Å (110). These peak positions, together with the noteworthy asymmetrical shape of the (200) reflection, are characteristic of turbostratic hexagonal birnessite (δ-$MnO_2$).

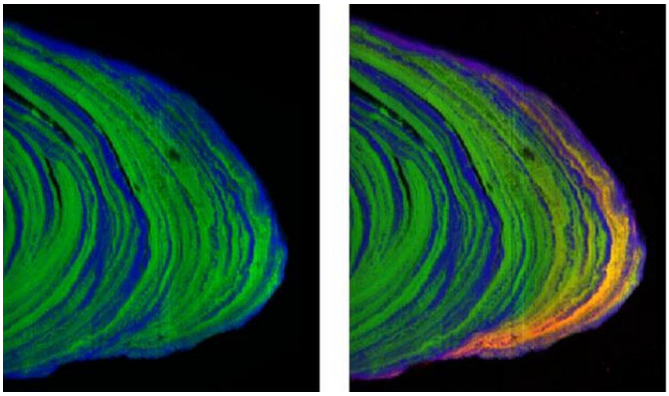

Figure 1. Synchrotron-based micro-X-ray radiation fluorescence (µSXRF) Fe and Mn maps of the outermost Fe and Mn layers of a ferromanganese nodule from the Baltic sea (6600 µm x 3780 µm, step size 15 µm, counting time 250 ms/pixel, red = Zn, green = Mn, blue = Fe, beamline: 10.3.2.). The onion-like structure of growth rims is clearly discernible as few hundreds µm thick Fe/Mn-rich bandings. Zn is exclusively associated with Mn, as indicated by the orange color of the Zn-containing Mn layers, and its concentration increases towards the surface.

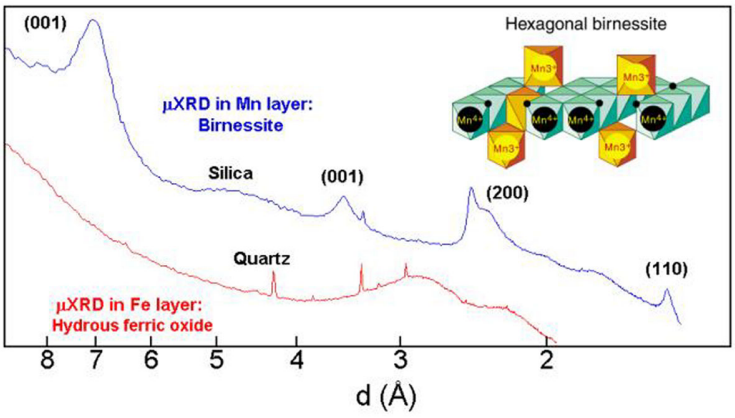


Figure 2. X-ray microdiffractograms collected in Mn (λ = 1.252 Å) and Fe (λ = 1.758 Å) layers. Mn is speciated as turbostratic hexagonal birnessite (δ-$MnO_2$), and Fe as hydrous ferric oxide. Quartz grains (sharp peaks) and silica particles (d ≈ 4.6 Å) were detected throughout the sample.

To determine the Zn sorption mechanism at the molecular-level, Zn K-edge µEXAFS spectra were collected in a Zn 'hot spot'. Qualitative information about the local structure of Zn can be obtained by comparing the unknown µEXAFS spectrum to reference EXAFS spectra from relevant model

compounds. The best spectral match was obtained with the Zn-sorbed birnessite reference, in which Zn is predominantly tetrahedrally, and secondarily octahedrally, coordinated and complexed above vacant sites of the manganese layer (Fig. 3). Comparison of radial structure functions (Fig. 3b) indicates that the Zn-O and Zn-Mn distances are both slightly, but significantly, shortened in the nodule sample, which is indicative of the presence of only $^{IV}$Zn. The preferred formation of the $^{IV}$Zn over the $^{VI}$Zn complex presumably arises from the presence of aliovalent $Mn^{3+}$ ions within the $MnO_2$ layer, because 4-fold coordinated Zn provides more positive charges to undersaturated oxygens (2+/4 = 0.5 v.u.) than a 6-fold coordinated Zn (2+/6 = 0.33 v.u.).

## CONCLUSION

This study demonstrates the merit of deploying in parallel fluorescence, diffraction, and absorption studies at micrometer scales of resolution. This unprecedented combination of techniques allows the determination of the structural form of trace elements in heterogeneous matrices with an unequaled precision. Since much of nature and synthetic materials are heterogeneous on micron and sub-micron length scales, we anticipate that the synergistic use of µSXRF, µSXRD, and µEXAFS will have broad applications and add to the arsenal of analytical methods available in environmental and materials science.

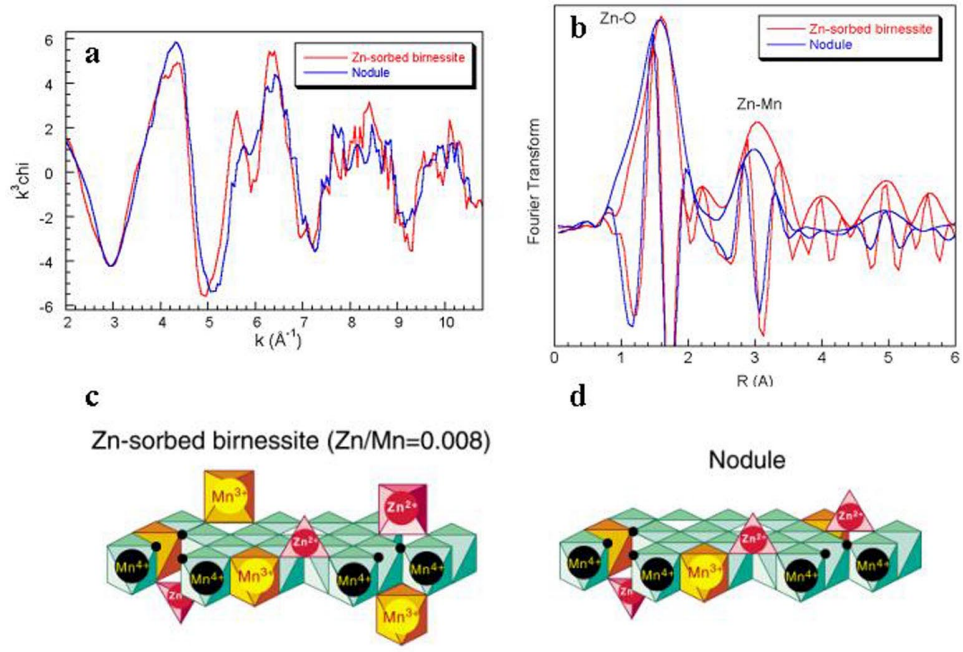


Figure 3. Zn K-dge µEXAFS spectrum and Fourier transform (modulus plus imaginary part) from a Zn 'hot spot' of the nodule rim presented in Fig. 1, compared to the Zn-edge data from a Zn-sorbed birnessite reference, in which Zn is sorbed as a mix of $^{IV}$Zn and $^{VI}$Zn complexes above vacant layer Mn sites. The unknown and reference data look similar, indicating that Zn are uptaken in a similar manner in the two compounds. However, Zn-O and Zn-Mn distances are clearly shorter in the natural sample because Zn is only four-fold coordinated.

This work was supported by the Director, Office of Energy Research, Office of Basic Energy Sciences, Materials Science Division, of the U.S. Department of Energy under Contract No. DE-AC03-76SF00098.

Principal investigator: Alain Manceau, Advanced Light Source, Ernest Orlando Lawrence Berkeley National Laboratory. Email: acmanceau@lbl.gov. Telephone: 510-643-2324.

# Strain and Stress in a Thin Film $YBa_2Cu_3O_x$ Bicrystal Grain Boundary on $SrTiO_3$ Substrate Studied by X-ray Micro-Diffraction

W.A. Caldwell[1], N. Tamura[1], R.S. Celestre[1], A.A. MacDowell[1], H.A. Padmore[1], and J.R. Patel[1,2]
[1]Advanced Light Source, Ernest Orlando Lawrence Berkeley National Laboratory,
University of California, Berkeley, California 94720, USA
[2]SSRL/SLAC, Stanford University, P.O. Box 43459, Stanford CA 94309, USA

## INTRODUCTION

Grain boundaries are important in the electrical transport properties of high-$T_c$ cuprate superconductors. $YBa_2Cu_3O_x$ superconducting devices take advantage of good transport behavior to make wires and use the poor transport (weak link) behavior to make Josephson junction devices [1]. Critical current densities are lower across the grain boundaries by orders of magnitude compared with the values in the bulk of single crystals [2]. The amount of misorientation of neighboring grains is an important parameter in determining the critical current density. In [001] tilt boundaries, one of the simplest grain boundaries, critical current densities drop markedly above 10 degrees [3]. High-resolution electron microscopy has shown that this misorientation angle, which corresponds to the transition from strong to weak intergrain coupling, occurs at the point of overlap of Cu-rich dislocation cores, indicating that the dislocation cores along the grain boundary are responsible for the weak-link behavior [4].

The purpose of this work is to probe the strain/stress of two $YBa_2Cu_3O_x$ bicrystal films near the grain boundary using x-ray microdiffraction in order to visualize the strain/stress fields caused by the dislocation cores at the grain boundary.

## EXPERIMENTAL

The samples consist of two $YBa_2Cu_3O_x$ bicrystal samples both with [001] tilt boundaries: one with a 36° tilt (high-angle, weak-link) boundary and the other with a 10° tilt (transition between strong coupling and weak-link) boundary. Both film samples are 260 nm thick and were deposited epitaxially in a controlled (high purity - $O_2$) environment on $SrTiO_3$ bicrystal substrates and post-growth oxygenated at 420° C for 1 hour prior to removal from the growth chamber.

Oxygen content of our samples were determined from $T_c$ measurements and then used to determine the stress free lattice parameters according to established reference relations [5]. White-beam Laue patterns in reflection mode at beamline 7.3.3 at the Advanced Light Source were taken and automatically indexed using a custom code (X-MAS) developed onsite. The X-ray microdiffraction end station on beamline 7.3.3 has the capability of providing high flux within a beam size of approximately 1 x 1 micron. Its setup has been described elsewhere [6].

## RESULTS

Measurements were taken in 1 micron steps to make a raster scan of 30 microns across the bicrystal grain boundary and 10 microns parallel to this boundary for both samples. Additionally, finer scans were made on the 10° sample with 0.5 micron steps of 10 microns by 10 microns and also with 0.25 micron steps of 2 microns by 2 microns. A sample diffraction pattern is shown in Figure 1. The geometrical parameters (sample-detector distance, center channel position and

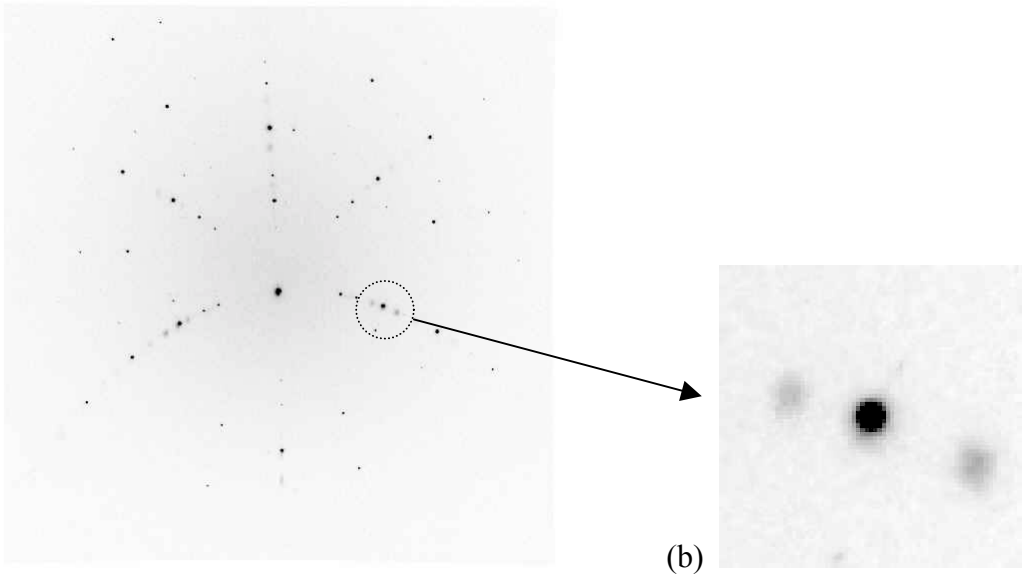


Figure 1. (a) White-beam Laue pattern of $YBa_2Cu_3O_7$ thin film on $SrTiO_3$ bicrystal substrate. (b) The most intense spots are due to the substrate (center of enlarged image). The fainter and more elongated spots are from the film (either side of central spot).

tilts of detector with respect to beam) were determined by using the $SrTiO_3$ substrate as an unstrained reference. $T_c$ measurements of 90.4 K yielded an $O_2$ content of 7.0, which was then used to calculate the bulk unstrained lattice parameters as: a = 3.8154 Å, b = 3.8888 Å and c = 11.6764 Å.

We found that the strain values in the $YBa_2Cu_3O_7$ film are on the order of $10^{-2}$ and the effect of the cubic substrate is to make the $YBa_2Cu_3O_7$ structure look tetragonal rather than orthorhombic. The values are consistent with epitaxial strains due to the difference in lattice parameters of the substrate and the film. Due to the large strain values, automated indexation of the diffraction pattern is not straight forward because of the necessity to use a large angular tolerance. We therefore used as an intermediate unstrained reference quadratic values for the $YBa_2Cu_3O_7$ lattice constants and then compare the refined values with the bulk reference. Figures 2 and 3 give the deviatoric strain along the crystallographic unit cell directions, a and b, averaged for the 10 traverses across the grain boundary in the 36° and 10° tilt samples, respectively.

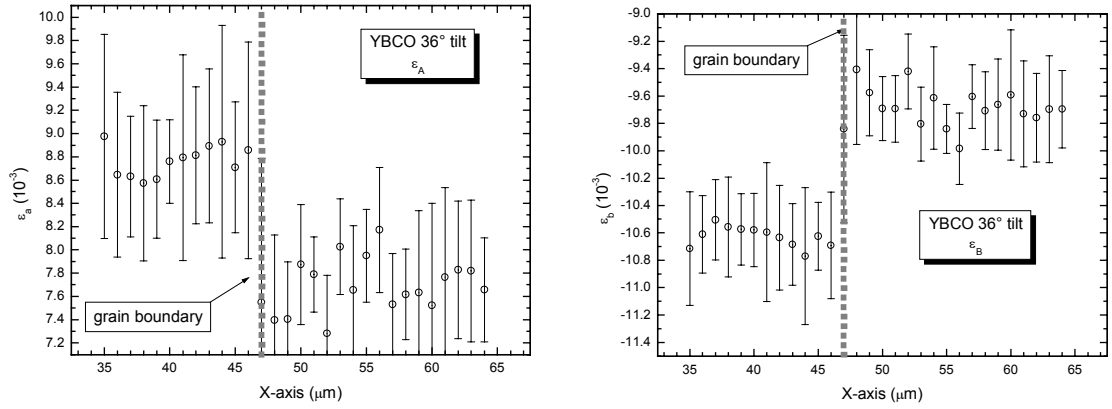


Figure 2. Deviatoric strain measurements along the a-direction (left) and the b-direction (right) of the unit cell averaged over 10 traverses across the grain boundary of the 36° tilt bicrystal.

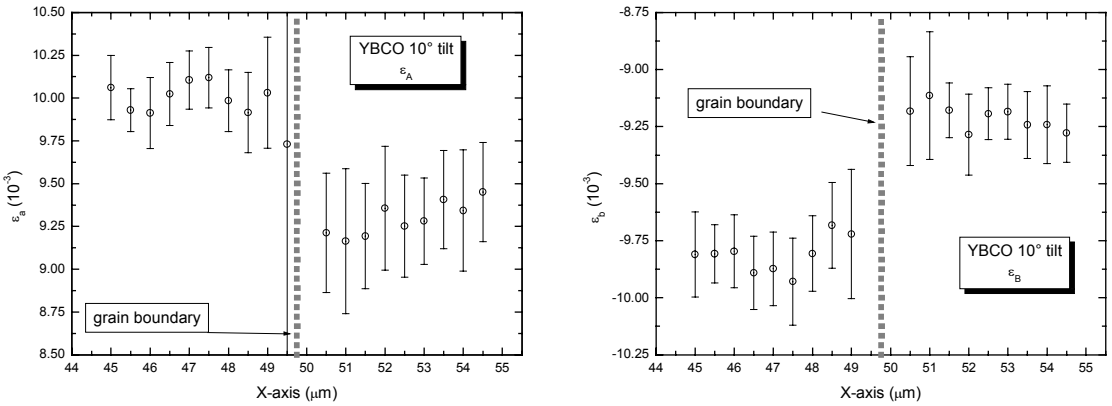


Figure 3. Deviatoric strain measurements along the a-direction (left) and the b-direction (right) of the unit cell averaged over 10 traverses across the grain boundary of the 10° tilt sample.

## CONCLUSIONS/DISCUSSION

The deviatoric strain state in the unit cell coordinate system is different on opposing sides of the 36° and 10° bicrystal grain boundary. No strain gradients can be detected within our spatial resolution limit as we approach the grain boundary from either side. Future work will include data collection and analysis at the cryogenic operating conditions of these films.

## ACKNOWLEDGMENTS

Thanks to Gertjan Koster and Ted Geballe for providing samples and measuring $T_c$'s.

## REFERENCES

1. J. Mannhart and P. Chaudhari, Physics Today **54**, 48 (2001).
2. P. Chaudhari et al., Phys. Rev. Lett. **60**, 1653 (1988).
3. D. Dimos, P. Chaudhari and J. Mannhart, Phys. Rev. B **41**, 4038 (1990).
4. Y. Gao et al., Physica C **174**, 1 (1991).
5. R. G. Munro and H. Chen, J. Am. Ceram. Soc. **79**, 603 (1996).
6. A. A. MacDowell et al., Nucl. Inst. Meth. A **467**, 936 (2001).

This work was supported by the Director, Office of Science, Office of Basic Energy Sciences, Materials Sciences Division, of the US Department of Energy under Contract No. DE-AC03-76SF00098 at Lawrence Berkeley National Laboratory.

Principal investigator: Wendel (Sander) Caldwell, Advanced Light Source, Ernest Orlando Lawrence Berkeley National Laboratory. Email: WACaldwell@lbl.gov. Telephone: 510-495-2233.